ACS OMEGA

http://pubs.acs.org/journal/acsodf

Article

Insights into the Distribution and Functional Properties of L-Asparaginase in the Archaeal Domain and Characterization of *Picrophilus torridus* Asparaginase Belonging to the Novel Family Asp2like1

Archana Sharma,[#] Vineeta Kaushik,[#] and Manisha Goel*

Cite This: *ACS Omega* 2022, 7, 40750−40765

Read Online

ACCESS | Metrics & More | Article Recommendations | Supporting Information

ABSTRACT: L-Asparaginase catalyzes the hydrolysis of L-asparagine to aspartic acid and ammonia and is used in the medical and food industries. In this investigation, from the proteomes of 176 archaeal organisms (with completely sequenced genomes), 116 homologs of L-asparaginase were obtained from 86 archaeal organisms segregated into Asp1, Asp2, IaaA, Asp2like1, and Asp2like2 families based on the conserved domain. The similarities and differences in the structure of selected representatives from each family are discussed. From the two novel archaeal L-asparaginase families Asp2like1 and Asp2like2, a representative of Asp2like1 family *Picrophilus torridus* asparaginase (PtAsp2like1) was characterized in detail to find its suitability in therapeutics. PtAsp2like1 was a glutaminase-free asparaginase that showed the optimum activity at 80 °C and pH 10.0. The Km of PtAsp2like1 toward substrate L-asparagine was 11.69 mM. This study demonstrates the improved mapping of asparaginases in the archaeal domain, facilitating future focused research on archaeal asparaginases for therapeutic applications.

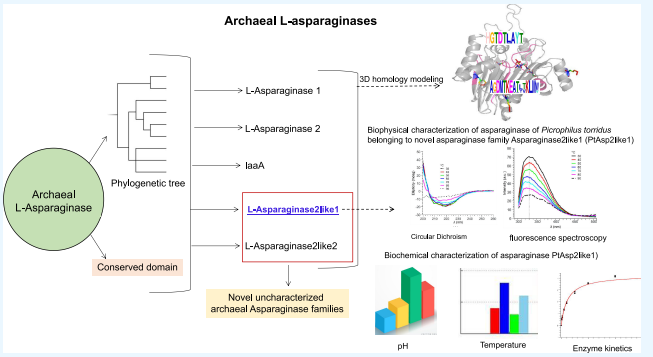

1. INTRODUCTION

Asparaginase (L-asparagine amidohydrolase; EC 3.5.1.1) catalyzes the hydrolysis of the amide group of the side-chain of L-asparagine, resulting in aspartic acid and ammonia. It is widely distributed in animals, plants, and microorganisms.[1] The enzyme is essential in the food and pharmaceutical sectors. Fungal ASNase is used in the food industry to inhibit acrylamide formation in heated food.[2,3] According to the International Agency for Research on Cancer (IARC 1994), this acrylamide is a probable carcinogen for humans. Novel improved ASNases with increased thermostability and activity across a broad pH range are in demand in the food industry.[4]

L-Asparaginase (ASNase) is used as an enzymatic chemotherapeutic agent in the multidrug treatment of lymphoid system malignancies, acute lymphoblastic leukemia (ALL), lymphosarcoma, Hodgkin's disease, melanosarcoma, etc.[1,5,6] Acute lymphoblastic leukemia (ALL) is a form of blood cancer primarily affecting children. The cancer cells exhibit a deficient synthesis of L-asparagine compared to normal cells and need an extracellular supply of L-asparagine to remain viable.[1] ASNase therapy reduces L-asparagine concentrations in the patient's plasma, thereby selectively starving the cancerous cells of this essential amino acid.[7] This therapy improves the patients' survival rates, but the side effects of the currently available therapeutic ASNase (from *Escherichia coli* and *Erwinia chrysanthemi*) include allergies and anaphylactic shock hepatotoxicity, which may limit its use in many patients.[8] The side effects primarily appear to be the outcomes of protein immunogenicity coupled with the L-glutaminase side activity, reducing the L-glutamine levels in plasma.[9−11] Therefore, the search for a better ASNase focuses not only on higher asparaginase activity but also on lower immunogenicity and the absence of L-glutaminase activity. Several reports in the literature propose additional prospects of this enzyme for developing medications for autoimmune diseases[12] and for treating infectious diseases such as scarlet fever, pharyngitis, necrotizing fasciitis, glomerulonephritis, toxic shock syndrome, etc.[13]

Currently, ASNases from *E. coli* and *Erwinia chrysanthemi* are commercially used in cancer therapy.[10,14−19] To reduce the immunogenicity problems associated with these commercial

Received: February 25, 2022
Accepted: March 31, 2022
Published: November 2, 2022

https://doi.org/10.1021/acsomega.2c01127
ACS Omega 2022, 7, 40750−40765

enzymes, the pegylated form of ASNase is available as pegaspargase (Oncaspar), which significantly reduced the immunogenicity and resided for a longer time in the bloodstream as compared to the native drug from *E. coli*.[7] But pegylated ASNase has certain drawbacks such as polydispersity, as pegylation is random,[20] and batch to batch variation, as PEG is randomly attached to the amino acid residue.[21−23] Some researchers reported a reduction in antibody production (*in vivo*) in animal models while using pegylated ASNase.[24] Despite these limitations, Oncaspar is commercially used as the first-line treatment of ALL in some countries.[25]

However, the search for new/novel ASNases with improved properties like reduced glutaminase activity, resistance to proteases, and less immunogenicity compared to the currently used ASNase is still going on. Brumano et al. (2019) reviewed in detail the significant problems with the presently available commercial ASNase and highlighted the need for biobetter ASNases.[25] Several reports on the development of biobetter ASNases using protein engineering, site-directed mutagenesis, PEGylation, bioconjugation, and immobilization are already available. Researchers have tried to identify the hotspot residues that might increase the substrate specificity of already available ASNases by site-directed mutagenesis, but such proteins are not commercially available yet.[26−28] Potential ASNase candidates from marine bacteria are also investigated for use in cancer therapy.[8]

ASNases known so far are divided into bacterial-type ASNases and plant-type ASNases. Bacterial-type ASNases are subdivided into type I and type II ASNases based on their cellular localization, substrate affinity and oligomeric structure.[8,29] Type I are cytosolic proteins with high Km for L-asparagine (Km in the millimolar range), while type II ASNases are secretory with lower Km (Km in the micromolar range).[30,31] Commercially, type II ASNases from bacteria are used in cancer therapy.[32] Both plant- and bacterial-type ASNases are structurally and evolutionary distinct from each other.[29] Plant-type ASNases from *E. coli* known as ECAIII/IaaA exhibit a higher affinity for isoaspartyl dipeptides as compared to L-asparagine.[29]

The archaeal protein repertoire, though unique, shares similarities with both eukaryotes and bacteria. This lends to the possibility that archaea may possess ASNases with high activity like bacteria and lower immunogenicity like human/eukaryotic proteins, along with unique features such as stability, selectivity, and lack of L-glutaminase activity. Archaeal organisms are generally regarded as safe since not even a single pathogenic organism has yet been identified from this kingdom. Archaeal enzymes are widely used in biotechnological and food applications because of their more agreeable biophysical properties such as thermostability and tolerance of extreme conditions. There are very few reports of ASNase characterization from archaeal organisms, mainly in archaea belonging to the genera *Pyrococcus* and *Thermococcus*.[33−40] But there appears to be no comprehensive study to collate probable archaeal ASNases or an effort to distinguish and differentiate these on the basis of their biochemical and biophysical properties.

In this study, we aimed to determine the occurrence and distribution of ASNase in the third domain, archaea. We used a data set of proteomes from the 176 archaeal organisms (with completely sequenced genomes available in NCBI) to hunt for the proteins similar to ASNases using the BLAST similarity search. A total of 116 homologs of ASNase were obtained from 86 archaeal organisms, and these were subjected to conserved domain database (CDD) analysis and motif analysis. Representatives from different archaeal ASNase families were subjected to 3D-structure homology modeling. The ASNase of *Picrophilus torridus* belonging to the novel family Asp2like1 was used as an archaeal representative for detailed biochemical and biophysical characterization to find its suitability in cancer therapy.

2. METHODS

2.1. Retrieval of Sequences. Proteomes from a total of 176 archaeal organisms (with completely sequenced genomes, available in NCBI as of Jan 2019) were used as a data set to search for ASNase homologs in archaea using the BLAST similarity search.[41] ASNase of *Picrophilus torridus* DSM 9790 was used as a seed sequence to run the BLAST similarity search with cutoff of $3e^{-12}$.

2.2. Multiple Sequence Alignment, Conserved Domain Analysis, and Phylogenetic Tree Construction. The keyword "asparaginase" was used to search the RCSB Protein Data Bank (RCSB-PDB) [https://www.rcsb.org/] for already available ASNase structures from bacteria, archaea, and eukaryotes. This was followed by a conserved domain database CDD v3.18-55570 PSSMs (https://www.ncbi.nlm.nih.gov/Structure/cdd/wrpsb.cgi)[42] search for finding the domain present in already known ASNases from bacteria, archaea, and eukaryotes whose structures are available along with proteomes from 176 archaeal organisms. The conserved domain analysis of ASNases whose structures are already available on RCSB-PDB from bacteria, archaea, and eukaryotes yielded a total of 133 structures of ASNases, including native ASNases, mutants, and ASNases with ligands (L-asparagine, L-glutamine). For phylogenetic tree construction, only native ASNases (available on RCSB-PDB) were selected and subjected to cd-hit at a sequence identity cutoff of 1.0 (http://weizhong-lab.ucsd.edu/cdhit_suite/cgi-bin/index.cgi)[43] and ClustalOmega[44] alignment to remove redundant ASNases, resulting in a data set of 34 sequences. Out of 176 archaeal proteomes from archaeal organisms used in this investigation, 116 homologs of L-asparaginase obtained from 86 archaeal organisms were used for phylogenetic analysis using MEGA 6.0 (Molecular evolution and Genetic Analysis). MEGA is an integral tool for sequence alignment, constructing the phylogenetic tree, and testing an evolutionary hypothesis[45] and is used to infer the phylogenetic relationship. The phylogenetic tree was constructed by the maximum likelihood (ML) method based on the gamma corrected Jones−Taylor−Thornton with bootstrapping of 1000 steps.

The amino acid sequences of archaeal representatives from five different families along with a few structurally and biochemically characterized ASNases from bacteria, eukaryotes, and archaea of Asp1, Asp2, and IaaA families were aligned using ClustalOmega.[44] The score of the alignment was checked by T-Coffee.[46]

2.3. Motif Analysis in Bacterial and Archaeal ASNase Protein Sequences. The conserved motif prediction among 116 archaeal ASNases along with the reported ASNases from bacteria and eukaryotes was performed using normal and discriminative mode of motif search using the MEME (Multiple Expectation−maximization for Motif Elicitation) server. The parameters were set as one motif per sequence and an expected motif length between 5 and 15 amino acids, with

https://doi.org/10.1021/acsomega.2c01127
ACS Omega 2022, 7, 40750−40765

other settings as default.[47] The conserved motif analysis within archaeal ASNase families was also performed using the MEME server with all other parameters same as above.

2.4. Structural Analysis of Selected ASNase Representatives from Different Archaeal Families. The representative organisms, each from five different archaeal ASNase families selected for homology modeling, were *Pyrococcus furiosus* (Asp1), *Haloferax volcanii* (Asp2), *Picrophilus torridus* (Asp2like1), *Sulfolobus tokodaii* (Asp2like2), and *Thermococcus onnurineus* (IaaA). All the 3D structures were predicted using SWISS-MODEL.[48] The crystal structure of *P. furiosus* ASNase is available at 2.50 Å resolution (PDB ID: 4Q0M);[39] therefore, it was directly used in the present study. The PDB IDs of templates used for homology modeling of representative ASNases were 4Q0M, 6PAB,[49] 4PVP,[50] 3C17,[51] and 2ZAK[52] for *P. furiosus*, *H. volcanii*, *P. torridus*, *S. tokodaii*, and *T. onnurineus*, respectively. The molecular graphic representations were prepared using the PyMOL molecular graphics system version 4.0.[53]

The active site and catalytic residues were identified and marked on modeled 3D structures of archaeal representatives selected from different ASNase families. An attempt was made to identify corresponding residues through primary sequence alignment followed by alignment of the 3D structure. As the crystal structure of *P. furiosus* ASNase of the Asp1 family (PfAsp1) is already reported, its active site residues were marked as reported by Tomar et al. (2014). In *Haloferax volcanii* ASNase of the Asp2 family (HvAsp2), active site residues were identified using *E. coli* ASNase of the Asp 2 family (ECAII) as a template.[54] The *P. torridus* ASNase of the Asp2like1 family (PtAsp2like1) was close to the human ASNase homolog; therefore, its active site residues were identified using hASNase3 as a template.[55] In *S. tokodaii* ASNase of the Asp2like2 family (StAsp2like2) and *T. onnurineus* ASNase of the IaaA family (ToIaaA), the active site residues were identified using plant-type ASNase in *E. coli* (ECAIII) as a template.[29,56]

2.5. Cloning, Expression, and Purification of PtAsp2-like1. The gene encoding the asparaginase protein (protein ID: NC_005877.1:c454513-453692) from *P. torridus* DSM 9790 was cloned in the pET28a(+) vector using restriction sites *Bam*H1 and *Xho*1 and expressed in the host *E. coli* BL21 (DE3). PtAsp2like1 was expressed in 500 mL of the LB medium containing 500 μg mL^{-1} kanamycin. The *E. coli* cells were grown to an optical density of 0.6 at 600 nm at 37 °C, and induction was done using IPTG (final concentration of 1 mM). The induced cells were grown for 5 h at 37 °C for ASNase expression. PtAsp2like1 was expressed as a 6× histidine-tagged fusion protein, and the recombinant enzyme was purified using Ni^{2+}-affinity chromatography. Cells were harvested by centrifugation at 8000*g* for 10 min. The centrifuged cell pellet was washed with a buffer (25 mM Tris−HCl buffer pH 8.0 and 100 mM NaCl) and then was resuspended in a lysis buffer (25 mM Tris−HCl buffer pH 8.0, 100 mM NaCl, 10% glycerol, and 0.2 mM PMSF). The cells were disrupted by sonication at 4 °C for 15 min (5 s on and 5 s off, amplification 30) using Vibra-Cell (Sonics, Connecticut, USA). The cell lysate was then centrifuged at 10,000*g* for 30 min at 4 °C to remove insoluble cell debris. The resultant supernatant was filtered through a 0.22 μm membrane (mdi: SY25KG-S) and loaded onto the 10 mL Ni^{2+}-NTA beads (G Biosciences) pre-equilibrated with a binding buffer (25 mM Tris−HCl buffer, 100 mM NaCl, pH 8.0). The unbounded proteins were washed with the binding buffer followed by a washing buffer (25 mM Tris−HCl buffer, 100 mM NaCl, 50 mM imidazole, pH 8.0) to remove weakly bound proteins. Then, the bound recombinant ASNase was eluted from the column with an elution buffer (25 mM Tris−HCl buffer, 100 mM NaCl, 250 mM imidazole, pH 8.0). The flow rate of the column was maintained at 1 mL min^{-1}. The eluted fractions were pooled and dialyzed overnight in a dialysis buffer (10 mM Tris−HCl, 10 mM NaCl, pH 8.0) at 4 °C. The dialyzed protein was loaded on to a Superdex column (Hi-Load 16/600 Superdex 200PG) equilibrated with a 10 mM Tris−HCl buffer with 5 mM NaCl. The column was washed with 2 column vol of the equilibration buffer. The flow rate for the size exclusion chromatography was set at 0.5 mL min^{-1}, and 10 mL fractions were collected. The protein concentration was determined by measuring A_{280} (extinction coefficient of protein = 13,410 M^{-1} cm^{-1} estimated from the amino acid composition) and the Bradford assay. For the Bradford assay, bovine serum albumin was used as a standard in the range of 10 to 100 μg mL^{-1}. For SDS-PAGE analysis, 10 μL of the protein sample was added to 10 μL of the SDS loading dye, and the mixture was heated at 100 °C for 5 min. The protein samples were stacked onto a 15% SDS polyacrylamide gel under reducing conditions. The gel was run at 80 V and was stained with Coomassie blue, and blue bands were imaged. The 3-Color Pre-stained Protein Ladder from Puregene (Genetix) was used. All the characterization studies were carried out with the 6× histidine-tagged enzyme without cleaving the tag.

2.6. Biophysical Characterization of PtAsp2like1 Using Circular Dichroism (CD) and Fluorescence Spectroscopy. The Online Protparam tool was used for estimating the number of aromatic amino acids in PtAsp2like1.[44] The aromatic amino acid composition of PtAsp2like1 includes 9 tyrosines, 12 phenylalanines, and no tryptophan. CD experiments were carried out in a Jasco J-815 spectropolarimeter with a Peltier-type temperature controller (Jasco CDF-426S/15). A quartz cell of 0.1 cm path length was used, and the data were collected under the following conditions: wavelength range, 200 to 260 nm; step resolution, 0.1 nm; time constant, 2 s; and scan speed, 100 nm/min. The spectral band width was kept constant at 2.0 nm. Three accumulations were recorded for each sample. For all CD experiments, 0.2 mg/mL protein was used and the concentration of the protein was estimated from the absorption at 280 nm (ε = 13,410 M^{-1} cm^{-1} evaluated from amino acid composition).

Temperature-mediated unfolding of PtAsp2like1 was performed at different temperatures from 30 to 90 °C. The reversibility of the unfolding process was studied by cooling the sample from 90 to 30 °C. The sample was incubated for 5 min at each temperature before recording the spectrum during heating and cooling. The changes in the secondary structure of protein were observed and noted.

To investigate the effect of pH on the secondary structure of PtAsp2like1, the protein was diluted in buffers of different pHs and incubated for 30 min. The buffers used for this study were 20 mM glycine HCl (pH 3.0), 20 mM acetate (pH 4.0 and 5.0), phosphate (pH 6.0 and 7.0), Tris chloride (pH 8.0), and glycine-NaOH (pH 9.0, 10.0, and 11.0). The effect of the denaturant on PtAsp2like1 was studied by incubating the protein for 1 h with different concentrations of guanidium hydrochloride (Gdn-HCl) (0−7 M) and urea (0−8 M), and changes in the protein conformation were recorded.

https://doi.org/10.1021/acsomega.2c01127
ACS Omega 2022, 7, 40750−40765

Using fluorescence spectroscopy, the temperature- and denaturant-mediated changes in the tertiary structure of PtAsp2like1 were elucidated. A Cary Eclipse spectrofluorimeter and quartz cuvette of 10 mm path length were used to record the fluorescence spectra. The protein sample was excited at 280 nm, and the emission spectra were recorded from 300 to 400 nm at room temperature. Excitation and emission slit widths of 5 nm each were used for this study. For all unfolding studies, the final protein concentration was 0.2 mg mL^{-1}.

2.7. Enzyme Assay. The ASNase activity was estimated by measuring the amount of ammonia released from the L-asparagine (substrate) hydrolysis reaction. The ASNase assay was performed according to Zuo et al. (2014). The enzyme assay mixture of 500 μL contained 0.02 M substrate L-asparagine, 25 mM Tris−HCl (pH 8.0), and 100 μL of the enzyme solution obtained after dialysis. The enzyme substrate reaction was performed at 37 °C and pH 8.0 for 5 min and was terminated by adding 100 μL of 1.5 M trichloroacetic acid (TCA). The reaction mixture was centrifuged at 12,000*g*, and 100 μL of the clear supernatant was added to 800 μL of deionized water and 100 μL of Nessler's reagent to measure the released ammonia after L-asparagine hydrolysis. All the measurements were done spectrophotometrically at 450 nm. The standard curve was prepared using ammonium sulfate in the range of 0.2 to 1.6 μmol mL^{-1} (1 mol of ammonium sulfate is equivalent to 2 mol of NH_4^+). A substrate control (reaction mixture containing the substrate and buffer), enzyme control (reaction mixture containing the enzyme and buffer), and buffer control (reaction mixture containing only the buffer) were used to account for the ammonia released, and the absorbance values were subtracted from the test. One unit (U) of L-asparaginase activity was defined as the amount of enzyme needed to release 1 μmol of ammonia per minute under the mentioned assay conditions. Glutaminase activity was measured using the same protocol, except that in place of L-asparagine, L-glutamine was used as a substrate.

2.8. Characterization of Enzyme and Kinetic Analysis. The effect of different temperatures on asparaginase activity was measured at different temperatures ranging from 30 to 100 °C. The pH of the reaction mixture was kept at 8.0.

The effect of different pHs on asparaginase activity was determined by measuring the enzyme activity at different pHs while keeping the reaction temperature 37 °C. The protein was incubated for 5 min in different pH buffers before estimating the enzyme activity. The buffers used for this experiment were 20 mM glycine HCl (pH 3.0), 20 mM acetate (pH 4.0 and 5.0), phosphate (pH 6.0 and 7.0), Tris chloride (pH 8.0), and glycine-NaOH (pH 9.0, 10.0, 11.0).

As this study was targeted to find asparaginases that can be used in cancer therapy, the kinetic parameters were measured at pharmacologically relevant conditions, viz., PBS buffer pH 7.2 and 37 °C. The substrate (asparagine) concentrations taken were 1, 2, 5, 10, 25, 50, 100, and 200 mM. The kinetic parameters Km, Vmax, kcat, and kcat/Km were calculated by nonlinear regression using the nls command in R 3.6.3.[57]

3. RESULTS

In the present investigation, a total of 176 completely sequenced archaeal proteomes were used as a data set to search for ASNase homologs using the BLAST similarity search (using *P. torridus* ASNase as a seed sequence). A total of 116 homologs of ASNase proteins were obtained from 86 different archaeal organisms.

3.1. Multiple Sequence Alignment, Conserved Domain Analysis, and Phylogenetic Tree Construction. Several studies have reported on the structure determination and characterization of ASNases from Asp1, Asp2, and IaaA families from bacteria[54,58−62] and eukaryotes.[55,62,63] Many ASNase structures are known from different bacteria with a main focus on *Escherichia* and *Erwinia* genus, as they are used commercially.[16,18]

The search for the keyword "asparaginase" on the RCSB Protein Data Bank (RCSB-PDB) [https://www.rcsb.org/] yielded a total of 133 structures of ASNase from bacteria, archaea, and eukaryotes till December 23, 2020. These 133 structures include ASNases with mutations and ligands like asparagine and glutamine (Table S1). We used the conserved domain database CDD v3.18-55570 PSSMs (https://www.ncbi.nlm.nih.gov/Structure/cdd/wrpsb.cgi) for finding the domain present in structurally characterized ASNases from bacteria, archaea, and eukaryotes along with 116 ASNase homologs present in 86 archaeal organisms. On the basis of the conserved domain present, all these ASNases were separated into different families (Table S2). The archaeal ASNases diversified into five different families, namely, Asp1, Asp2, IaaA, Asp2like1, and Asp2like2 (Table 1). The Asp1, Asp2, and IaaA families of archaeal ASNases were similar to bacteria. However, Asp2like1 and Asp2like2 are putative uncharacterized archaeal ASNase families with no known crystal structure in RCSB-PDB. The bacterial ASNases separated into different families such as Asp1, Asp2, ansA, ansB, IaaA, and L-asparaginase_like family. *E. coli* possesses ASNase from families ansA (ECAI), ansB (ECAII), and IaaA (ECAIII). ASNases from *Homo sapiens* and *Cavia porcellus* belong to *the* ASRGL1_like ASNase (cd04702) family named metazoan L-asparaginase type-2 and are members of the ntn_asparaginase_2_like superfamily (cd04512). This superfamily is also shared by Asp2like1 (cd04703) and Asp2like2 (cd14950) families. Structures of ASNases from *Wolinella succinogenes, Helicobacter pylori,* and *Erwinia carotovora* are available that belong to Asp2/type II bacterial ASNases (cd08964). *E. coli* and *Erwinia* ASNases belonging to type II (periplasmic) ASNases are used commercially for the treatment of acute lymphoblastic leukemia.[10,14−19]

The crystal structures of only Asp1 family ASNases are available from few archaeal organisms such as *Pyrococcus horikoshii, Pyrococcus furiosus* and *Thermococcus kodakarensis.*[33,39,40] Asp1 family ASNases have a low affinity for L-asparagine, as seen from their high Km. ASNases from *P. horikoshii,*[33] *P. furiosus,*[34] *T. kodakarensis* (TK1656)[36] displayed asparaginase activity with no glutaminase side activity, while *T. gammatolerans* EJ3 ASNase contains glutaminase side activity, with a high Km for L-asparagine.[37] To the best of our knowledge, no crystal structures or homology modeled structures are available from archaeal ASNases belonging to different ASNase families, except Asp1. The phylogenetic tree was made using 116 ASNase homologs from archaea (present study) along with native structures of ASNases from bacteria, archaea, and eukaryotes (structures taken from RCSB-PDB). The archaeal ASNases separated into five different clusters—Asp1, Asp2, IaaA, Asp2like1, and Asp2like2−on the phylogenetic tree (Figure S1). Bacterial ASNases of Asp2, ansB, and L-asparaginase_like families formed a separate outgroup cluster but were found close to archaeal Asp2

https://doi.org/10.1021/acsomega.2c01127
ACS Omega 2022, 7, 40750−40765

Table 1. Description of Different Families of ASNase in Archaea[a]

subfamily	CDD domain ID	description	reference
Asp1	cd08963/smart00870/COG0252/pfam00710	type1 (cytosolic) bacterial ASNase. Highly specific for asparagine, are localized in cytosol, and act as a dimer. Catalytic threonine is the conserved residue.	https://www.ncbi.nlm.nih.gov/Structure/cdd/wrpsb.cgi
Asp2	cd08964/smart00870/pfam00710	type 2 (periplasmic) bacterial ASNase. This family of ASNase is highly specific to asparagine and localized in the periplasm. They act as tetramers and are dimers of two dimers with threonine as a catalytic residue.	https://www.ncbi.nlm.nih.gov/Structure/cdd/wrpsb.cgi
IaaA	COG1446/cd04512/pfam01112	isoaspartyl peptidase/ECAIII. Initially classified as a plant-type ASNase based on sequence homology and ASNase activity. Currently known primary function is hydrolysis of isoaspartyl dipeptides.	https://www.ncbi.nlm.nih.gov/Structure/cdd/wrpsb.cgi[51]
Asp2like1	cd04703	uncharacterized subfamily of ASNase type 2-like enzymes. The proenzymes of this family undergo autoproteolytic cleavage before a threonine residue to produce alpha and beta subunits. The threonine becomes the N-terminal residue of the beta subunit and a catalytic residue.	https://www.ncbi.nlm.nih.gov/Structure/cdd/wrpsb.cgi
Asp2like2	cd14950	an uncharacterized subfamily of ASNase type 2-like enzymes. The proenzymes of this family undergo autoproteolytic cleavage before a threonine residue to produce alpha and beta subunits. The threonine becomes the N-terminal residue of the beta subunit and a catalytic residue.	https://www.ncbi.nlm.nih.gov/Structure/cdd/wrpsb.cgi

[a]On the basis of conserved domain analysis, archaeal ASNases were grouped into five different families.

homologs. Archaeal ASNases of Asp1, Asp2like2, and IaaA families formed separate clusters on the tree. Bacterial and eukaryotic ASNases also formed separate clusters.

3.2. Motif Analysis in Bacterial and Archaeal ASNase Protein Sequences. The discriminative motif analysis revealed the presence of common and unique motifs in bacterial and archaeal ASNase protein sequences. In the Asp2 family, motif ^{81}HGTDT^{85} is highly conserved in bacterial and archaeal ASNase protein sequences. In the Asp2 family, both bacterial and archaeal ASNase protein sequences share one common motif, ^{9}GGTIA^{13}, while motif ^{81}HGTDT^{85} is present only in homologs of ASNase in archaea and not found in bacteria. Motif ^{106}KPVV^{109} is unique to bacterial ASNase protein sequences of Asp2 family and is not seen in archaeal homologs of the same family. In the IaaA family, two motifs, ^{87}RVGD^{90} and ^{48}FNAG^{51}, are present in archaeal ASNases but absent in bacteria homologs. Asp2like1 and Asp2like2 are two uncharacterized families of archaeal ASNase, and the conserved motifs present in ASNase homologs of these families are given in Table 2. The unique and distinct motifs present in ASNase protein sequences in bacteria and ASNase homologs found in archaea are shown in Table 2.

The amino acid sequence alignment of selected archaeal representatives from five different ASNase families along with a few structurally characterized ASNases from bacteria, archaea, and eukaryotes of Asp1, Asp2, and IaaA families was performed. It was observed that ASNase from *Picrophilus torridus* of the Asp2like1 family (PtAsp2like1), *Sulfolobus tokodaii* ASNase of the Asp2like2 family (StAsp2like2), and *Thermococcus onnurineus* ASNase of the IaaA family (ToIaaA) were close to the plant-type ASNase from *E. coli* (PDB ID: 2ZAK, 2ZAL),[52] *Homo sapiens* (PDB ID: 4O0C),[55] and *Cavia porcellus* (PDB ID: 4O47)[62] ASNases. ASNases from *Pyrococcus furiosus* of the Asp1 family (PfAsp1) aligned with known ASNases of the Asp1 family, and ASNases from *Haloferax volcanii* of the Asp2 family (HvAsp2) aligned with known ASNases of the Asp2 family (Figure S2).

The distribution of 116 ASNase homologs from 86 archaeal organisms in different archaeal order was also studied, and it was seen that only Asp2like2 family ASNases were found in the proteomes of Thermoproteales, Sulfolobales, Desulfurococcales, and Acidilobales. In contrast, Asp2like1 family ASNases were present only in the proteomes of Thermoplasmatales (Table 3).

3.3. Structural Analysis of Selected ASNase Representatives from Different Archaeal Families. The amino acid sequence identity among representative archaeal ASNases from each of the five families is shown in Table S3A. The topology diagram illustrates the mutual orientation and arrangement of secondary structure elements in all representative archaeal ASNases of different families. The topology diagram clearly shows distinct N- and C-terminal domains linked by a flexible loop in PfAsp1 and HvAsp2, while this was not observed in ToIaaA, PtAsp2like1, and StAsp2like2 (Figure 1A). The monomeric structure of ToIaaA, PtAsp2like1, and StAsp2like2 was superimposed, and it was observed that these three archaeal ASNases were structurally related to each other, while PfAsp1 and HvAsp2 were closer to each other (Figure 1B,C). This was further validated by comparing the RMSD values of these selected representative archaeal ASNases (Table S3B). Based on common motifs and structural similarity, Asp1 and Asp2 are grouped together (named group 1 ASNase in this study), while Asp2like1, Asp2like2, and

https://doi.org/10.1021/acsomega.2c01127
ACS Omega 2022, 7, 40750−40765

Table 2. Conserved and Unique Motifs in Bacterial and Archaeal ASNase Protein Sequences[a]

Asp1 family	^{81}HGTDT^{85}	^{65}SINY^{68}	^{51}DSTLIQPEDW^{60}	^{89}DMTKEAT^{95}	^{66}GVDL^{69}
bacteria	+	+	−	−	−
archaea	+	+	+	+	+
Asp2 family	^{81}HGTDT^{85}	^{9}GGTIA^{13}	^{106}KPVV^{109}		
bacteria	−	+	+		
archaea	+	+	−		
IaaA family	^{87}RVGD^{90}	^{48}FNAG^{51}		^{161}VGAV^{164}	
bacteria	+	+		+	
archaea	+	+		+	
	Motifs in uncharacterized ASNase family in archaea				
Asp2like1	^{87}RVGD^{90}	^{48}FNAG^{51}	^{176}STGG^{179}	^{161}VGAV^{164}	
archaea	+	+	+		
Asp2like2	^{87}RVGD^{90}		^{176}STGG^{179}	^{161}VGAV^{164}	
archaea	+		+	+	

[a]The numbering of the motif in Asp1 and Asp2 family archaeal ASNase homologs is according to PfAsp1. In bacterial ASNases of the Asp2 family, the numbering is according to 3ECA (PDB ID). In ASNases belonging to IaaA, Asp2like1, and Asp2like2 families, the numbering of the motif corresponds to *P. torridus* of the Asp2like1 family.

Table 3. ASNase Families Present in Different Archaeal Orders[a]

		ASNase family				
phylum	order	Asp1	Asp2	Asp2like1	Asp2like2	IaaA
Euryarchaeota	Thermococcales	+				+
Crenarchaeota	Thermoproteales				+	
Crenarchaeota	Sulfolobales				+	
Crenarchaeota	Desulfurococcales				+	
Crenarchaeota	Acidilobales				+	
Euryarchaeota	Thermoplasmatales			+		
Euryarchaeota	Halobacteriales		+	+		+

[a]Archaeal ASNases were mainly distributed in two phyla: Euryarchaeota and Crenarchaeota.

IaaA form another group (named group 2 ASNase in this study). These two groups also differ in their catalytic residues.

3.3.1. Structural Analysis of Pyrococcus furiosus of the Asp1 Family (PfAsp1). The crystal structure of PfAsp1 is available at 2.50 Å resolution (PDB ID: 4Q0M).[39] PfAsp1 is 327 amino acids in length. It belongs to the Asp1 family, and three distinct motifs M1 (^{46}DLKNV**DSTLIQPEDW**^{60}), M3 (^{287}A G **D M T K E** A T V T **K L M** W^{301}), and M4 (^{159}SRD**AFESINYP**IIA**E**^{173}) differentiate Asp1 from the other families. The modeled structure is composed of 9 α-helices and 14 mixed β-sheets. The four antiparallel β-sheets are located in the N-terminal domain (Figure 2A). The putative active site residues are T11, S52, T53, T83, D84, K154, and Y273 (Figure 2D,E). Among these active site residues, T11, T83, D84, K154, and Y273 are catalytically important residues. Most of the active site residues are present on the N-terminal domain. The catalytic residues threonine T83 and D84 lie within motif M2, and Y273 lies on motif M5 (Figure 2B). The active site residues are present on the surface of the protein due to which the substrate-binding cavity looks wide and open (Figure 2C).

3.3.2. Structural Analysis of Haloferax volcanii of the Asp2 Family (HvAsp2). HvAsp2 (WP_004043218.1) is 324 amino acids in length. The homology model was generated using *E. coli* Asp2 as a template (PDB ID: 6PAB, sequence identity 34.85%).[64] The distinct motif M4 (^{3}PQ**V**TVLST**GGTIAS**T^{17}), which includes the highly conserved GGTI motif, is characteristic of the Asp2 family and distinguishes it from the other ASNase families. HvAsp2 is modeled as a homotetramer, the significant characteristic of this family. The structure is composed of 11 helices and mixed beta sheets. The three antiparallel beta sheets are present in the N-terminal domain (Figure 3A). The putative active site residues are T13, S26, T87, D88, K161, S55, and G277, and all of them are present on the N-terminal domain except G277 (Figure 3D,E). The catalytically important threonine residues T87 and T13 are part of motif M1 and M4, respectively. D88 and K161 are part of motif M1 and M2, respectively (Figure 3B). The catalytic residues are T13, S26, T87, D88, K161, and G277 (Figure 3E). The active site residues are present on the surface of the protein due to which the substrate binding cavity looks wide and open (Figure 3C).

3.3.3. Structural Analysis of Picrophilus torridus of the Asp2like1 Family (PtAsp2like1). PtAsp2like1 (WP_048059440.1) is 273 amino acids in length. The homology model was generated using human ASNase as a template (PDB ID: 4PVP, sequence identity 35.47%).[50] Motif M4 (^{209}**TGVGEE**IIKNM**L**CIS^{223}) differentiates the Asp2like1 family from other ASNase families. A clear division of the monomeric structure of PtAsp2like1 into N- and C-terminal domains was not seen, as observed in PfAsp1 and HvAsp2. Each monomer comprises 10 alpha helices and mixed beta sheets (4 antiparellel and 2 flanking) (Figure 4A). The active site residues are H7, G8, G9, N49, T159, T177, R187, D190, T209, G210, and G212 (Figure 4D,E). Among these, R187 and D190 are the part of motif M1; N49 is part of motif M2; T209, G210, and G212 lie within motif M4; and T177 is the part of motif M5 (Figure 4B). Most of the active site residues lie within the motifs and are highly conserved. T160, T177, and T209 are catalytic residues (Figure 4E). The active site

https://doi.org/10.1021/acsomega.2c01127
ACS Omega 2022, 7, 40750−40765

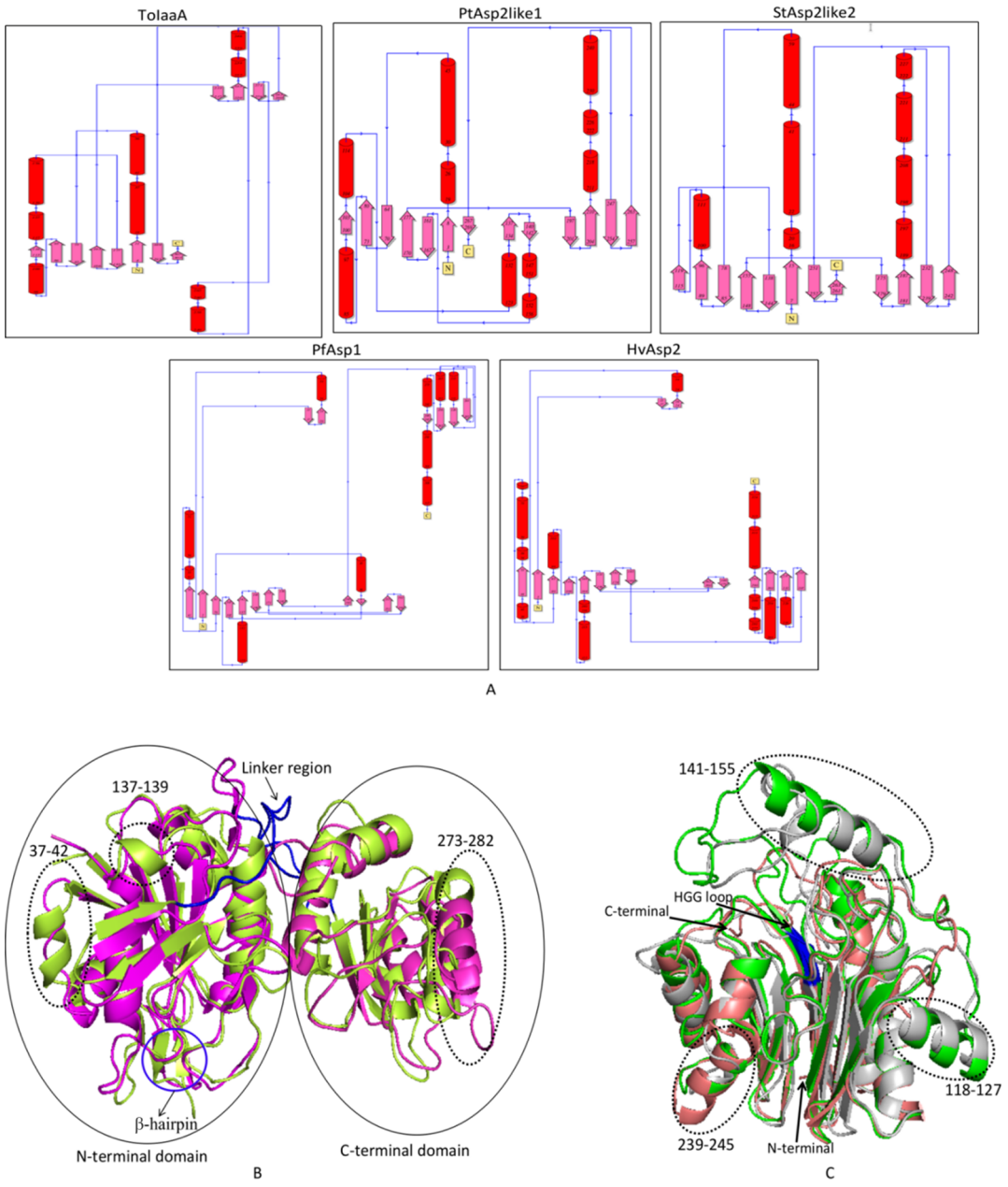

Figure 1. (A) Topology diagram showing the secondary structural arrangement of all representative archaeal ASNases selected from five families. (B) Superimposition of PfAsp1 (magenta) and HvAsp2 (lemon). The distinct regions are shown in dotted circles (black). The linker region connecting the N and C domains is shown in blue. β-Hairpin is circled in blue color. N- and C-terminal domains are circled in solid black. (C) ToIaaA (green), PtAsp2like1 (gray), and StAsp2like2 (deep salmon) are superimposed with dissimilar regions shown in black dotted circles and the HGG loop shown in blue. N- and C-terminal ends are indicated by arrows.

pocket appears to be tunnel-shaped with active site residues buried inside (Figure 4C).

3.3.4. Structural Analysis of Sulfolobus tokodaii of the Asp2like2 Family (StAsp2like2). StAsp2like2 (WP_010979894.1) is 271 amino acids in length. The homology model was generated using *E. coli* L-Asp as a template (PDB ID: 3C17, sequence identity 36.36%).[51] There is no unique motif that differentiates the Asp2like2 family from other families. The monomeric structure of StAsp2like2 is not divided into N- and C-terminal domains. Each monomer comprises seven alpha helices and mixed beta sheets (five antiparallel and two flanking) (Figure 5A). The active site residues are G13, A14, D63, G135, D136, T137, T155, G157, R165, D168, T187, G188, and G190 (Figure 5D,E). Some of these residues, such as R165, D168, T155, and T137, lie within the motifs and are highly conserved (Figure 5B). T137, T155, and T187 are catalytic residues (Figure 5E). The active site pocket appears to be tunnel-shaped with active site residues buried (Figure 5C).

3.3.5. Structural Analysis of Thermococcus onnurineus of the IaaA Family (ToIaaA). ToIaaA (WP_012572354.1) is 306 amino acids in length. The homology model was generated using *E. coli* L-Asp as a template (PDB ID: 2ZAK, sequence identity 38.61%).[52] The monomeric structure of ToIaaA is also not divided into N- and C-terminal domains. Each monomer comprises eight alpha helices and mixed beta sheets (five antiparellel and two flanking) (Figure 6A). The active site residues are G8, G9, A10, G11, T12, L53, F59, P57, I58, D55,

https://doi.org/10.1021/acsomega.2c01127
ACS Omega 2022, 7, 40750−40765

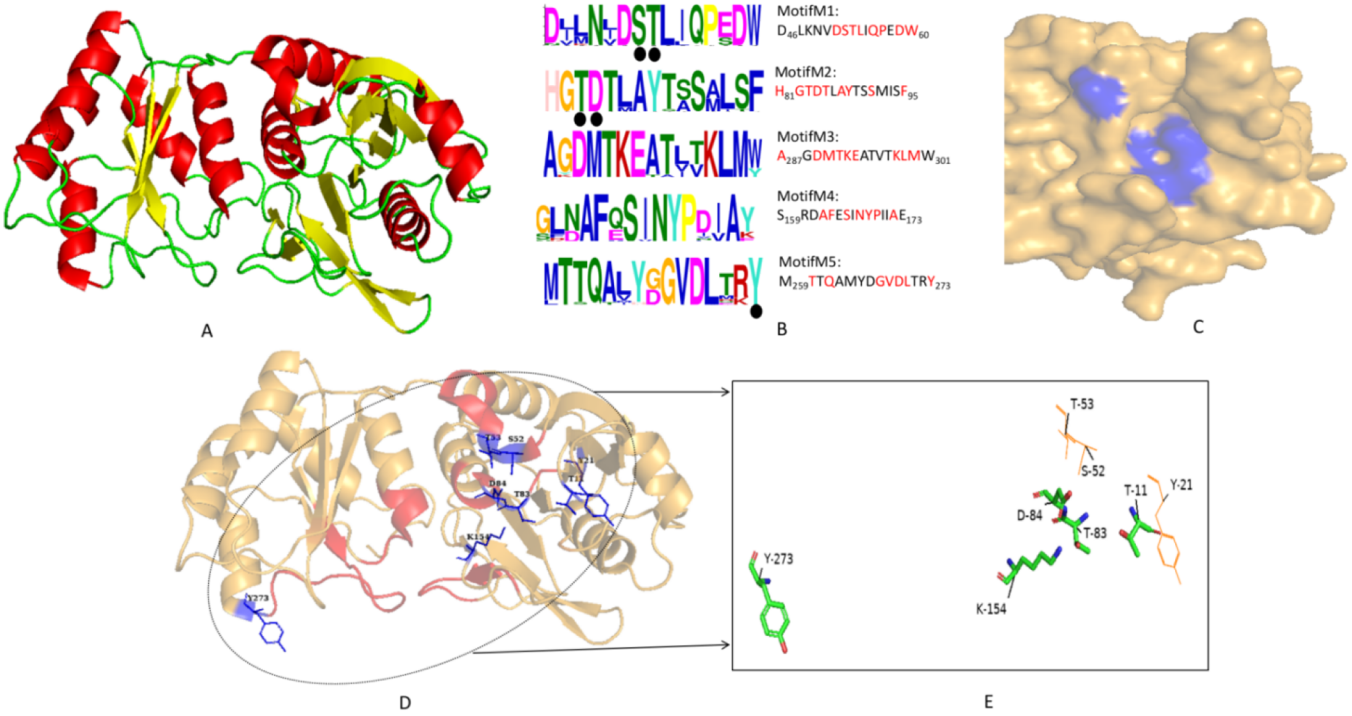

Figure 2. Structural analysis of PfAsp1 (4Q0M). (A) Cartoon diagram of PtAsp1 showing alpha helices (red), beta sheets (yellow), and loops (green). (B) Motifs predicted in the Asp1 family. The active site residues within the motif are shown as black circles below the residue. (C) The surface diagram of PfAsp1 with substrate binding cavity is shown in blue. (D) Cartoon diagram of PfAsp1 with motifs in red color and active site residues shown as sticks in blue (E) Active site residues. Catalytic residues are shown as sticks, while other active site residues are shown as orange lines.

N60, A61, G62, T63, T176, T193, G194, G195, R203, D206, T225, G226, G228, and S291 (Figure 6D,E). Residues F59 and N60 are part of motif M3, and T176 is part of motif M5 and is conserved (Figure 6B). The catalytic residues are T176, T193, and T225 (Figure 6E). The active site pocket appears to be tunnel-shaped with active site residues buried (Figure 6C).

3.4. Cloning, Expression, and Purification of PtAsp2-like1+. The recombinant PtAsp2like1 was expressed in fusion with a C-terminal 6× histidine-tag, leading to a single-step purification using nickel affinity column chromatography. The enzyme purified by affinity chromatography showed three bands on SDS-PAGE, indicating that the protein existed in cleaved and uncleaved forms. The molecular weight of the purified enzyme was estimated to be approximately 32 kDa by SDS-PAGE and was consistent with the theoretical value calculated from the predicted amino acid sequence. This 32 kDa protein got cleaved into two bands of 22 and 12 kDa as seen on the SDS-PAGE (Figure S3A). The gel filtration analysis also showed a single peak (Figure S3B), and SDS PAGE analysis of the corresponding peak fraction showed three bands of 32, 22, and 12 kDa (Figure S3C) indicating the possibility that two populations of protein might be present uncleaved and partially cleaved.

3.5. Biophysical Characterization of PtAsp2like1 Using Circular Dichroism (CD) and Fluorescence Spectroscopy. Circular dichroism and fluorescence spectroscopy are used for the biophysical characterization of proteins. Fluorescence spectroscopy estimates the tertiary structure of a protein, and far-UV CD spectrum is used to scan the secondary structure of the protein. The far UV-CD spectra were recorded at various temperatures, and it was observed that the secondary structure of PtAsp2like1 remained stable up to 70 °C. The secondary structure of the protein was lost entirely at 90 °C, indicating the unfolding of the protein (Figure S4A). On cooling the heat-denatured protein, the native structure was not regained; this suggests that the unfolding of the protein was irreversible (Figure S4B). Steady-state fluorescence studies at different temperatures were performed to study the thermal unfolding of PtAsp2like1. A gradual decrease in the fluorescence intensity on increasing temperature from 30 to 90 °C was observed. The λmax of the protein remained constant at 320 nm (Figure S4C).

The effect of pH on the secondary structure of PtAsp2like1 was studied over a wide pH range using far-UV CD. It was observed that at pH 2 and 3, there were significant conformational changes in the secondary structure of PtAsp2-like1. In the pH range of 4 to 11, the PtAsp2like was stable with no change in the secondary structure (Figure S4D).

The effect of intrinsic fluorescence spectroscopy showed that at pH 2.0 and 3.0, a blue shift in λmax was observed from 320 to 310 nm, indicating the significant conformational changes at these pHs. There was no change in fluorescence intensity and λmax in the pH range of 4.0−11.0, suggesting the stability of PtAsp2like1 in this pH range (Figure S4E).

The chemical (urea and Gdn-HCl) mediated unfolding of the PtAsp2like was carried out. The CD spectroscopy analysis showed that at low Gdn-HCl concentrations of 0.25 and 0.5 M, the protein was stabilized in the presence of the denaturant (Figure S5A). It is already reported that a lower concentration of the denaturant stabilizes the protein.[65] The ellipticity at 222 nm was gradually increased with increasing Gdn-HCl concentration (Figure S5B). On increasing Gdn-HCl beyond 2 M concentration, there were changes in the secondary

https://doi.org/10.1021/acsomega.2c01127
ACS Omega 2022, 7, 40750−40765

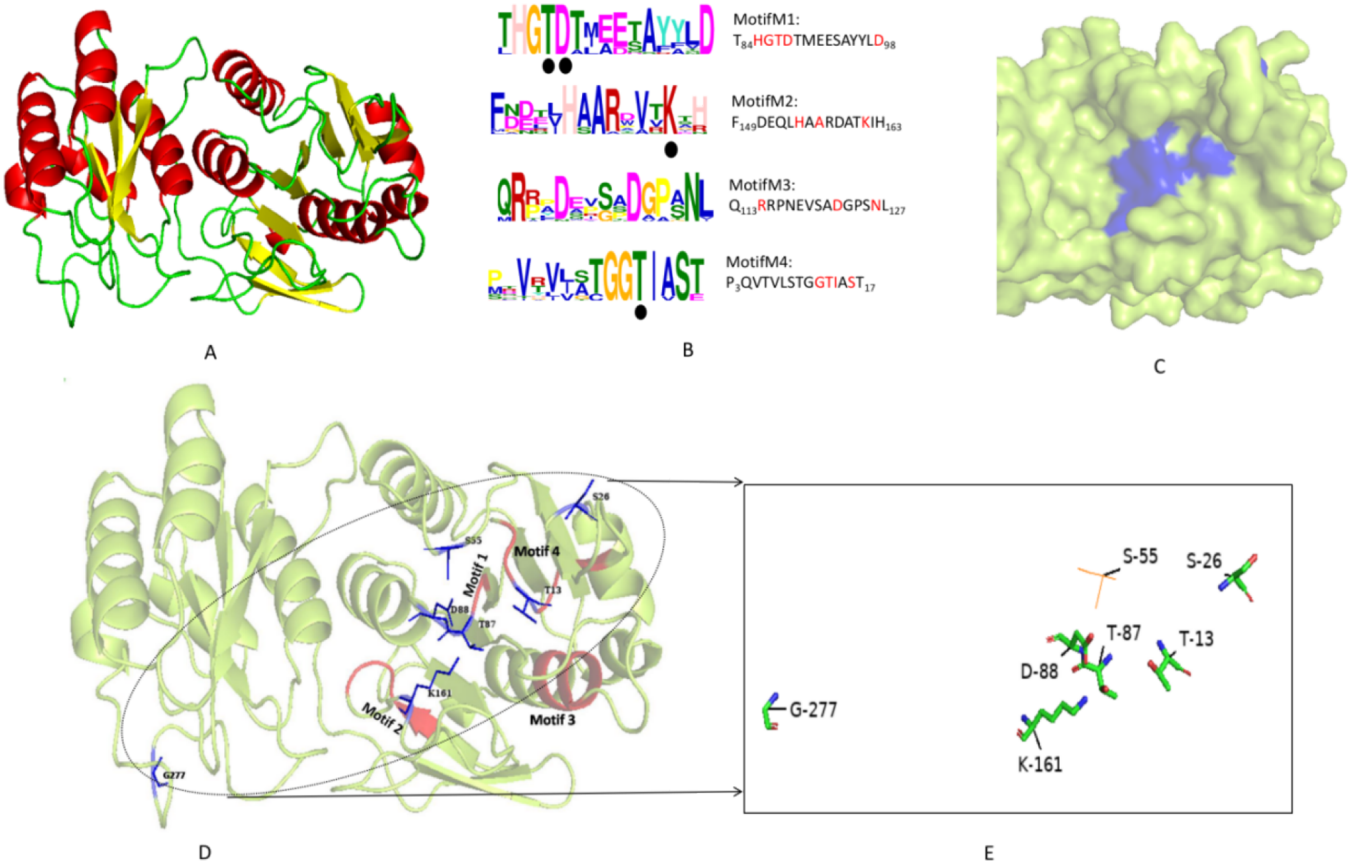

Figure 3. Structural analysis of HvAsp2 using template 6PAB (PDB ID). (A) Cartoon diagram of PtAsp1 showing alpha helices (red), beta sheets (yellow), and loops (green). (B) Motifs present in the Asp2 family. The active site residues that lie within the motif are shown as black circles below the amino acid residue. (C) Surface diagram of HvAsp2 with substrate binding cavity shown in blue color. (D) Cartoon diagram of HvAsp2 with motifs in red color and active site residues shown as sticks in blue. (E) Active site residues. Catalytic residues are shown as sticks, while other active site residues are shown as orange lines.

structure with a completely unfolded structure at 7 M Gdn-HCl (Figure S5A).

The fluorescence spectroscopy showed that a low concentration of Gdn-HCl (0.1 and 0.5 M) stabilized PtAsp2like1 as indicated by an increase in fluorescence intensity and no change in λmax (Figure S5C,D). On increasing the Gdn-HCl concentration beyond 1 M, there is a decrease in fluorescence intensity. At a higher concentration of Gdn-HCl, two different peaks were observed at 320 and 360 nm, indicating a significant change in the conformational state of the protein (Figure S5C).

CD data showed little change in the PtAsp2like1 secondary structure up to 3 M urea concentration. A change in ellipticity was noticed on increasing the urea concentration with a significant change in the secondary structure conformation from 5 M urea concentration. The intrinsic emission fluorescence data also showed a decrease in fluorescence intensity and blue shift in wavelength at high urea concentrations (4 to 8 M), indicating changes in the tertiary structure of the protein in the presence of high concentrations of urea (Figure S6).

3.6. Characterization of Enzyme and Kinetic Analysis.

The asparaginase activity was estimated in the temperature range of 30 to 100 °C. The enzyme activity increased gradually with the increase in temperature from 30 to 80 °C. The optimum activity of the enzyme was displayed at 80 °C with a drastic drop in asparaginase activity beyond 80 °C (Table 4).

The asparaginase activity was monitored in the pH range of 2.0 to 11.0, and it was observed that there is no asparaginase activity in the extreme pH range, i.e., pH 1.0 to 3.0. From pH 4.0 to 10.0, there is a gradual increase in asparaginase activity with the optimum activity at pH 10.0. There is a slight difference in enzyme activity in the pH range of 4.0 to 11.0 (Table 5).

3.6.1. Enzyme Kinetics. The kinetic properties of PtAsp2-like1 were assessed at pH 7.2 and 37 °C (pharmacologically relevant conditions) in the presence of substrate L-asparagine. The Km of the PtAsp2like1 toward substrate L-asparagine was calculated to be 11.69 mM. The kcat and catalytic efficiency of PtAsp2like1 were 5.6×10^{-2} s^{-1} and 0.47×10^{-2}, respectively.

4. DISCUSSION

Very few studies on archaeal ASNases are available, limiting our knowledge to only Asp1 family ASNases from archaea; therefore, a detailed investigation was carried out to study the occurrence and distribution of ASNases in archaea.

A data set of 176 available archaeal proteomes was used to search for ASNase homologs in the archaeal domain. Out of 176 completely sequenced proteomes from archaeal organisms, 116 homologs of ASNase were obtained (which belong to 86 archaeal organisms). These archaeal homologs were further separated into five different families on the basis of conserved domain present. Apart from the three well-known families of ASNase, namely, Asp1, Asp2, and IaaA, several archaeal

https://doi.org/10.1021/acsomega.2c01127
ACS Omega 2022, 7, 40750−40765

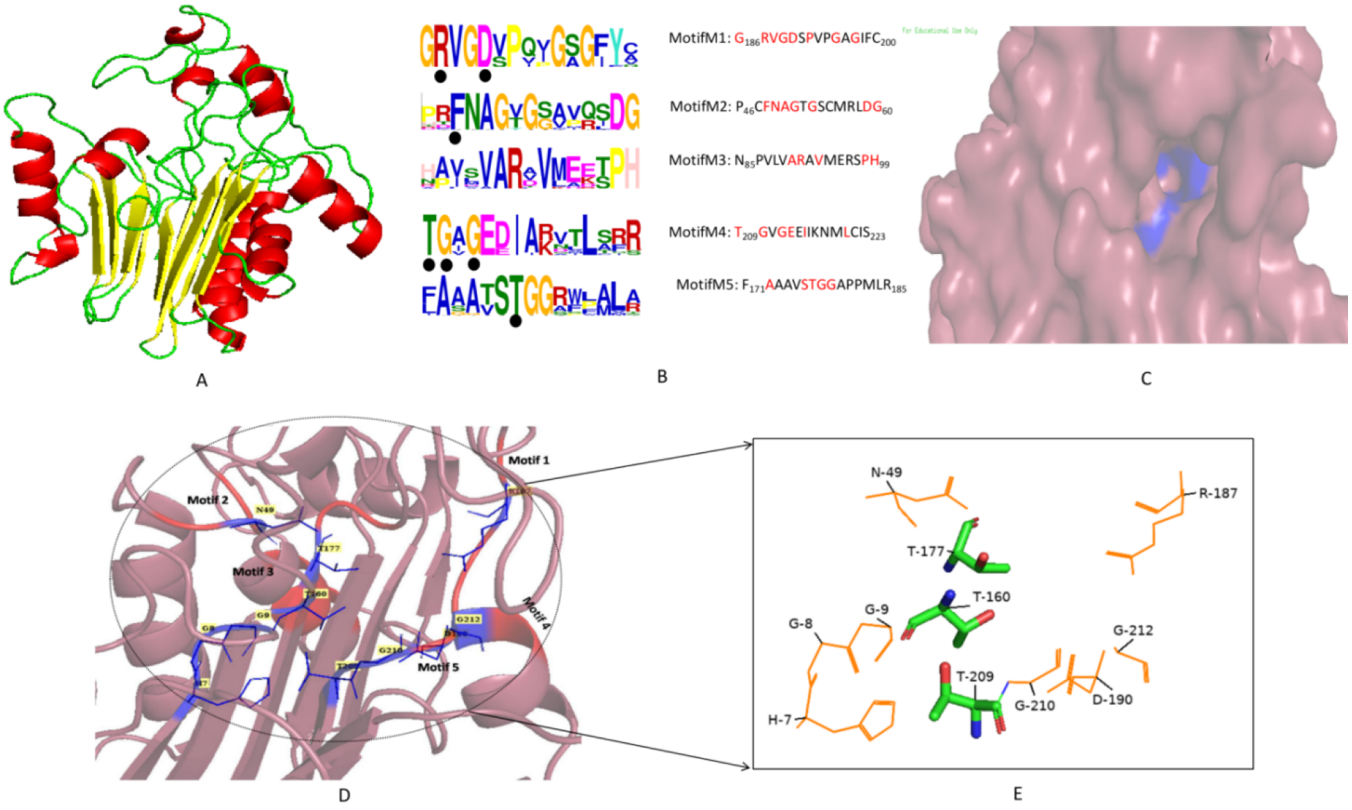

Figure 4. Structural analysis of PtAsp2like1 using template 4PVP (PDB ID). (A) Cartoon diagram of PtAsp1 showing alpha helices (red), beta sheets (yellow), and loops (green). (B) Motifs present in Asp2like1 family. The active site residues that lie within the motifs are shown as black circles below the residue. (C) Surface diagram of PtAsp2like1 with substrate binding cavity shown in blue color. (D) Zoomed view of substrate binding cavity with motifs in red color and active site residues shown as sticks in blue color. (E) Active site residues. Catalytic residues are shown as sticks, while other active site residues are shown as orange lines.

ASNase homologs clustered with uncharacterized putative ASNase families like Asp2like1 and Asp2like2. The distribution of these ASNases in different archaeal orders showed that only Asp2like2 ASNases were found in the proteomes of Thermoproteales, Sulfolobales, Desulfurococcales, and Acidilobales, while only Asp2like1 ASNases were found in the proteomes of Thermoplasmatales. Archaeal Asp2like1, asp2-like2, and IaaA orthologs form a separate branch of the tree. The Asp1 family ASNases from bacteria and archaea segregated on the phylogenetic tree. *Homo sapiens* and *Cavia porcellus* ASNases are members of the ASRGL1_like family, with none of the archaeal ASNases used in the present study belonging to this family. However, archaeal ASNases of IaaA, Asp2like1, and Asp2like2 families along with ASNases from *Homo sapiens* and *Cavia porcellus* share a common superfamily (cd04512).

The amino sequence alignment showed a clear distinction between ASNases of different families. Most of the catalytic residues are well conserved within each family. Motifs ^{7}HGG^{9}, ^{48}FNAG^{51}, ^{161}VGAVA^{165}, ^{176}STGG^{179}, and ^{87}RVGD^{90}, all containing catalytically active residues, are conserved across group 2 ASNases. In group 1 ASNases, β-hairpin is present in the N-terminal domain, which is similar to the active site flexible loop in Asp2 ASNase reported from bacteria and Asp1 ASNases from archaea.[33,60,64] In group 2 ASNases, the ″HGG″ loop probably corresponds to the β-hairpin of group 1 ASNases as it is also located in the N-terminal region of the protein and close to the active site. This loop in both ASNase groups is highly mobile and considered to modulate the substrate entry and probably acts as a ″gatekeeper″ responsible for the specificity of ASNase for a particular substrate. The active site residues T11 (PfAsp1 numbering) located on ″β-hairpin″ and G8 and G9 present on the ″HGG″ loop suggest the involvement of the loop in catalysis. The functional role of the ″HGG″ loop in the autoproteolytic cleavage of the enzyme and asparaginase activity is already suggested by Nomme et al. (2014). Similarly, β-hairpin is also known to play a significant role in the initiation of catalysis.[33,55]

The overall structures of all the archaeal ASNase representatives used in this study are similar, composed of nearly equal α-helices and β-sheets, consistent with the previous reports. The amino acid lengths of all selected representatives are also close, indicating no change in protein length during the evolution. Representative archaeal ASNases were taken from each of the five families for homology modeling. Based on RMSD values, the homology model structure of group 1 ASNases is related, and group 2 ASNases are structurally similar. However, the homology model structure of representatives across two groups was significantly different. All archaeal representative ASNases were modeled as dimers except HvAsp2. The Asp2 family ASNases are reported as homotetramers, described as dimers of dimers.[58] The crystal structures of only Asp1 family ASNases are known from archaea, which form homodimers and do not associate as homotetramers.[33,34,36,39,40] PfAsp1 (4Q0M) used as the Asp1 representative from archaea *P. furiosus* is a dimer.[38] It is reported that a dimer unit is sufficient for enzyme activity.[33] PtAsplike1, StAsp2like2, and ToIaaA were modeled as

https://doi.org/10.1021/acsomega.2c01127
ACS Omega 2022, 7, 40750−40765

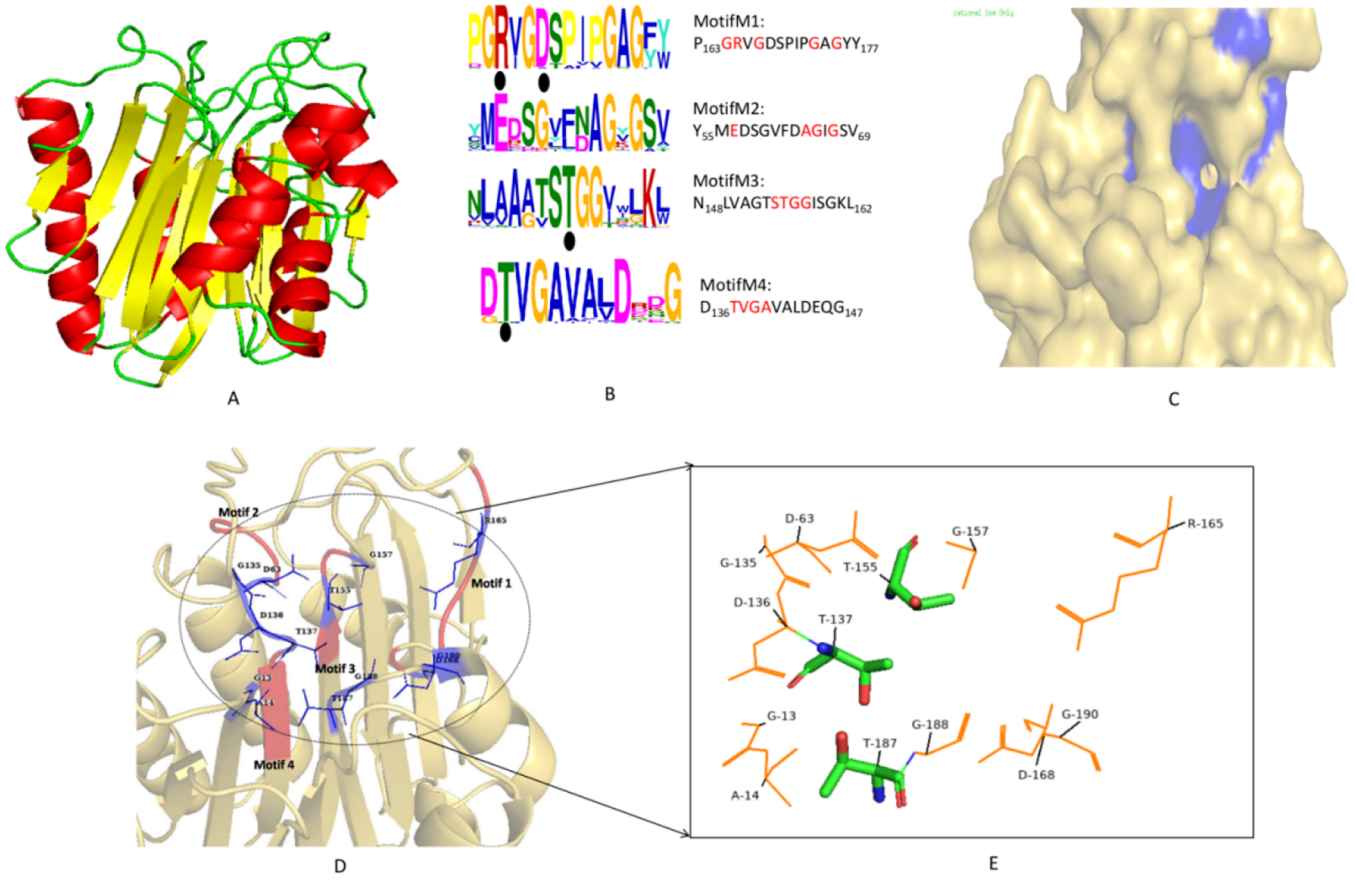

Figure 5. Structural analysis of StAsp2like2 using template 3C17 (PDB ID). (A) Cartoon diagram showing alpha helices (red), beta sheets (yellow), and loops (green). (B) Motifs present in the Asp2like2 family. The active site residues within the motif are shown as black circles below the residue. (C) Surface diagram of StAsp2like2 with substrate binding cavity shown in blue color. (D) Zoomed view of substrate binding cavity with motifs marked in red color and active site residues shown as sticks in blue color. (E) Active site residues. Catalytic residues are shown as sticks, while other active site residues are shown as orange lines.

homodimers, indicating the possibility that, in most of the archaeal ASNases, probably dimer is the minimum unit that possesses all the necessary conditions for enzyme activity. All of the group 2 ASNases were superimposed with each other but showed structural variability in some regions (Figure 3B,C). Significant variations were observed in region 141−155 (amino acid residues). In PtAsp2like1 and ToIaaA, this region is made up of a helix, while in StAsp2like2, this region is modeled as a loop.

It is believed that the bacterial-type enzymes have a disordered active site that is correctly organized on substrate binding. However, plant-type enzymes, like other Ntn-hydrolases, undergo autoproteolytic cleavage before activation.[56]

In Asp1 and Asp2 family ASNases, the active site is thought to be composed of two catalytic triads: I and II. Ortlund et al. (2000) proposed an alternative triad made up of residues T12, Y25, and E283 in ECAII.[66] This arrangement was debated, as Y25 cannot act as base chemically and residue E283 essential residue in this mechanism only assists in substrate binding and is dispensable in catalysis.[67] However, Tomar et al. (2014) reported the existence of two catalytic triads in *P. furiosus* ASNases of the Asp1 family. It has been reported that the function of triad I in the acylation of substrate L-asparagine is to form an enzymatic intermediate and the function of triad II in the deacylation of the intermediate in the presence of a water molecule is to release L-aspartic acid and ammonia as products of the enzymatic reaction.[39] These two catalytic triads are thought to function as an independent acid−base−nucleophile machinery in a sequential mode.[66,68] In *Pyrococcus furiosus* ASNase, in catalytic triad I, two of the residues that were found to interact with the substrate were T11 (nucleophile) and D84 (acid) from the N-terminal domain, while the third residue Y273 (base) was from the C-terminal domain. The triad II residues D84 (acid), K154 (base), and T83 in PfAsp2 carry out the deacylation reaction in the presence of activated water.[39] The catalytic mechanism of the *Haloferax volcanii* ASNase homolog in archaea belonging to the Asp2 family selected as one of the representatives for homology modeling was compared with EcaII (*E. coli* type II ASNase).[39] In HvAsp2, the catalytic machinery also appears to be divided into two triads (I and II), similar to ECAII (PDB ID 3ECA). The triad I residues of ECAII are T12, Y25, and E283, where T12 and Y25 are present in the N-terminal domain and E283 comes from the C-terminal domain. The triad II residues are D90, K162, and T89, all present in the N-terminal domain. The catalytic site in HvAsp2 appears to be similar to ECAII, made up of triads I and II, with all the putative catalytically important residues conserved except S26 (Y25 in ECAII) and G277 (E283 in ECAII), which are different from ECAII. Residue Y25 in ECAII is part of the mobile loop that closes the active site during catalysis. Therefore, this variable loop region was missing from the sequence alignment. In HvAsp2, S26 was seen in place of Y25

https://doi.org/10.1021/acsomega.2c01127
ACS Omega 2022, 7, 40750−40765

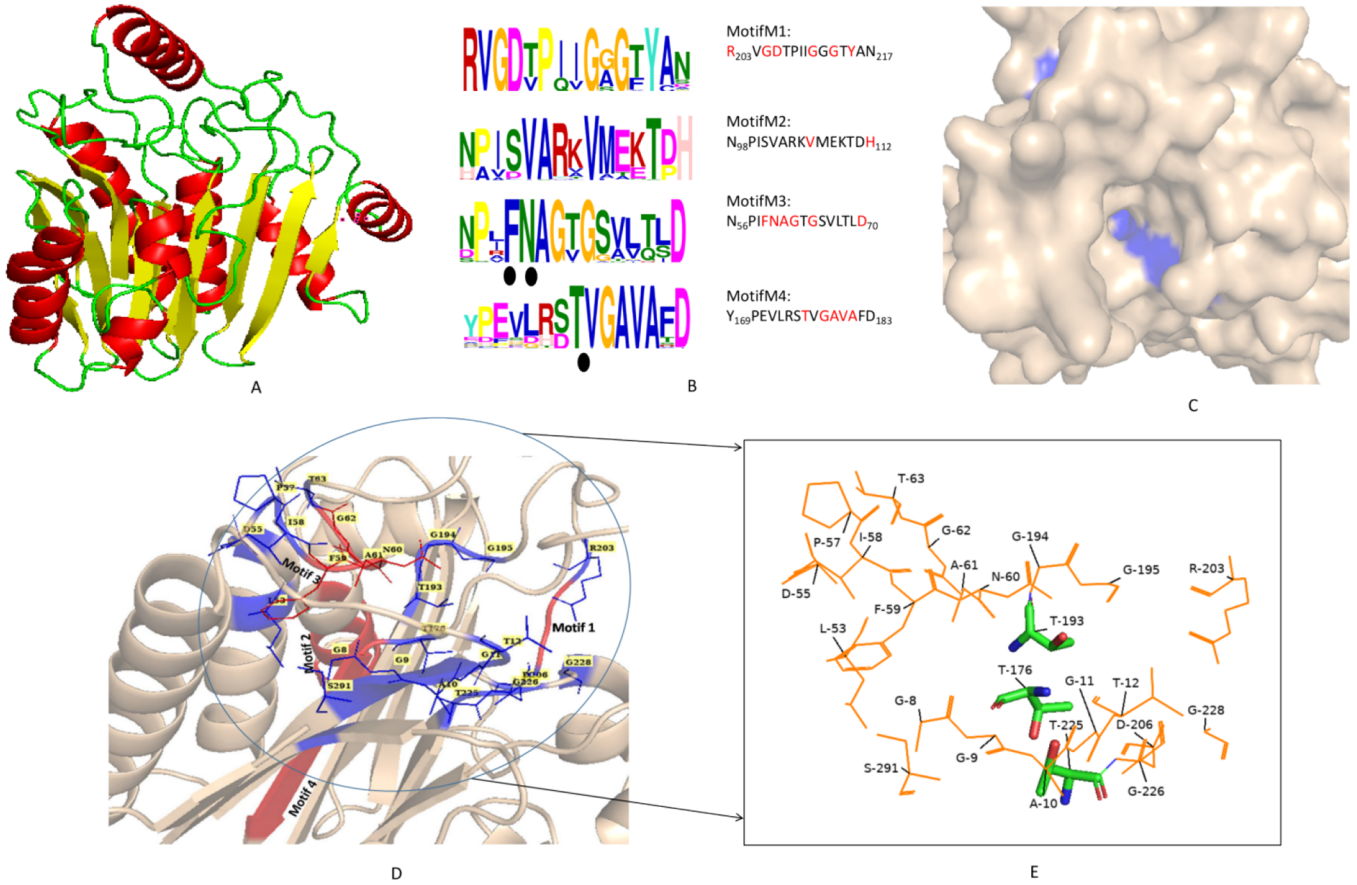

Figure 6. Structural analysis of ToIaaA using template 2ZAK (PDB ID). (A) Cartoon diagram showing alpha helices (red), beta sheets (yellow), and loops (green). (B) Motifs present in IaaA family. The active site residues that lie within the motif are shown as black circles below the residue. (C) Surface diagram of ToIaaA with substrate binding cavity shown in blue color. (D) Zoomed view of substrate binding cavity with motifs marked in red color and active site residues shown as sticks in blue color. (E) Active site residues. Catalytic residues are shown as sticks, while other active site residues are shown as orange lines.

Table 4. Effect of Temperature on ASNase Activity[a]

temperature (°C)	asparaginase activity (U/mL) ± SE	relative asparaginase activity (%)	*P* value (two-tailed unpaired *t* test, *n* = 3)
30	4.90 ± 0.24	28.2	
40	7.05 ± 0.32	40.5	.0058
50	8.39 ± 0.41	48.3	.0616
60	11.13 ± 0.50	64.0	.0133
70	12.91 ± 0.29	74.3	.0369
80	**17.37 ± 0.67**	**100**	**.0036**
90	8.22 ± 0.39	47.3	.0003
100	8.20 ± 0.35	47.2	.9714

[a]The *t* test was carried out between the activities at adjacent temperatures on the scale. Lower *P* values show higher significant difference.

Table 5. Effect of pH on Asparaginase Activity[a]

pH	asparaginase activity(U/mL) ± SE	relative asparaginase activity (%)	*P* value (two-tailed unpaired *t* test, *n* = 3)
2.0	0	0	
3.0	0	0	
4.0	0.28 ± 0.01	12.2	.0001
5.0	0.57 ± 0.02	25	.0002
6.0	1.42 ± 0.05	62.2	.0001
7.0	1.75 ± 0.06	76.7	.0134
8.0	2.03 ± 0.06	89.0	.0299
9.0	1.98 ± 0.03	86.8	.4975
10.0	**2.28 ± 0.09**	**100**	**.0341**
11.0	1.58 ± 0.04	69.2	.0021

[a]The *t* test was carried out between the activities at adjacent pH on the scale. Lower *P* values show higher significant difference.

in the alignment as well as homology model. Both serine and tyrosine are polar in nature, while glutamic acid is charged and glycine is hydrophobic.

Plant-type asparaginases are members of the N-terminal nucleophile (Ntn) hydrolase family.[69,70] Proteins from this family are synthesized as a single polypeptide precursor that lacks enzyme activity and only after autoproteolytic cleavage enzyme becomes active. The autocleavage mechanism is thought to be different between different classes of Ntn enzymes.[50] Plant-type ASNases are reported from humans[55] and bacteria.[51] In human ASNases, the threonine triad (Thr168, Thr186, and Thr219) is present, and its role in autoproteolytic cleavage and substrate hydrolysis is already elucidated by Nomme et al. (2014).[55] In group 2 ASNases, the threonine triad participates in catalysis and is conserved in archaeal ASNase representatives of families IaaA (ToIaaA: T176, T193, and T225), Asp2like1 (PtAsp2like1: T160, T177, and T209), and Asp2like2 (StAsp2like2: T137, T155, and T187), which are close to human, *Cavia porcellus*, and plant-

https://doi.org/10.1021/acsomega.2c01127
ACS Omega 2022, 7, 40750−40765

type ASNases. The autoproteolytic cleavage mechanism and function of the threonine triad in Asp2like1 and Asp2like2 ASNases are still unexplored. Based on available reports and its structural similarity to plant-type ASNases, it can be assumed that its catalysis mechanism might be similar to them. The active site pocket as can be seen from the surface diagram is similar in group 1 ASNase, while in group 2 ASNase, the substrate binding cavity appears to form a tunnel-like structure. These differences in the structure of substrate binding cavity and active site residues might be responsible for the different substrate selection and variable Km for asparaginase activity.

ASNases from two archaeal genera, *Pyrococcus* and *Thermococcus*, are structurally and biochemically characterized,[33,36,37] with all of them belonging to the Asp1 family.[33,36−38] All the characterized ASNases from archaea are thermostable with the pH optimum in the alkaline range.[34,36,37]

Asp2 family ASNases are periplasmic with both asparaginase and glutaminase activity, and bacterial ASNases (ASNases from *E. coli* and *Erwinia*) of this family are used commercially for the treatment of ALL.[10,14−19] But these commercially available ASNases have certain shortcomings.[9−11] Many researchers have tried to eliminate or reduce the glutaminase side activity of bacterial ASNases of the Asp2 family by site-directed mutagenesis without significantly affecting ASNase activity.[27,28] In these studies, catalytically important residues were untouched, while other residues close to the binding pocket or involved indirectly in substrate binding or product release were mutated.[71,72] Some were able to achieve improvements in terms of reduced glutaminase activity without affecting ASNase activity.[54,71] It is desired to obtain ASNases with improved properties such as glutaminase-free ASNases, resistance to proteases, thermostability, improved shelf life, and reduced immunogenicity. This can be achieved either by improving the existing ASNases by protein engineering[25] or by screening new ASNases. New ASNase variants with all the desired properties are not yet available.[25] So, mining the third domain archaea might be helpful in searching biobetter ASNases. The phylogenetic analysis of bacterial and archaeal ASNases of the Asp2 family (present study) clearly shows no direct correlation between bacterial and archaeal ASNases. The amino acid sequence alignment of archaeal ASNase of the Asp2 family HvAsp2 and *E. coli* ASNase (PDB ID: 6PAB) of the same family showed little sequence identity of only 34.85%. Both bacterial and archaeal Asp2 family ASNases show similar catalytic architecture and tetrameric structure. These observations indicate the possibility of convergent evolution. IaaA or plant-type ASNases from *E. coli* are closely associated due to their high sequence similarity with plant ASNases and their ability to hydrolyze isoaspartyl dipeptidase.[60,73,74] They showed a relatively lesser affinity for L-asparagine as compared to bacterial Asp2 family ASNases.[74] The IaaA/plant-type ASNase from bacteria has only been studied in detail from *E. coli*. Archaeal families Asp2like1 and Asp2like2 are completely unexplored with no report in the literature.

Based on our *in silico* analysis, we found two new/novel archaeal ASNase families: Asp2like1 and Asp2like2. Homology modeling of representatives from these two families showed a similar structure. Therefore, a representative from one of these families (Asp2like1) was selected for biochemical and biophysical characterization. *Picrophilus torridus* is a thermoacidophilic archaeon isolated from solfataric fields of northern Japan and grows optimally in extreme conditions such as 60 °C and pH 0.7.[75] The gene encoding asparaginase protein was cloned and heterologously expressed with IPTG induction. The enzyme was purified using affinity and gel filtration chromatography. The enzyme purified after gel filtration chromatography showed a single peak. Its SDS analysis resulted in three bands, indicating that the protein might have existed in cleaved and uncleaved forms. There is a possibility that cleaved parts of the protein are still attached, resulting in one single peak, as seen in the gel filtration chromatogram. This can be correlated with the studies on human ASNase reported by Nomme et al. (2014). It is reported that bacterial L-asparaginases are purified in fully cleaved/active form as compared to human asparaginase, which is purified as inactive uncleaved protein.[55] PtAsp2like1 was purified in active form and no chemical treatment was needed for its activation, as observed in the case of human ASNase. The purified PtAsp2like1 displayed activity toward substrate L-asparagine, while no activity was observed in the presence of substrate L-glutamine. This suggests that PtAsp2-like1 is a glutaminase-free L-asparaginase, which is one of the desired characteristics required in ASNase for its application in cancer therapy, as glutaminase side activity leads to several side effects.[9−11]

Circular dichroism and fluorescence spectroscopy were used for the biophysical characterization of proteins. Fluorescence spectroscopy estimates the tertiary structure of a protein, and far-UV CD spectrum is used to scan the secondary structure of the protein. The far UV-CD spectra were recorded at various temperatures, and it was observed that the secondary structure of PtAsp2like1 remained stable up to 70 °C and that, at 90 °C, the protein was completely unfolded. The unfolding of the protein was irreversible as the native structure of the protein was not regained on cooling (Figure 3B).

Steady-state fluorescence studies showed a gradual decrease in the fluorescence intensity on increasing the temperature from 30 to 90 °C. Fluorescence is a radiative process involving the transfer of electrons from the first excited triplet state to the ground state. Therefore, on increasing temperature, the rate of emission of photon by the nonradiative processes such as internal conversion increases, resulting in a decrease in the fluorescence emission intensity.[76]

PtAsp2like1 was stable in the pH range of 4 to 11 as monitored through far-UV and steady-state fluorescence spectroscopy. This can also be correlated with no change in ellipticity at 222 in CD studies and, similarly, no change in fluorescence intensity and λmax in fluorescence studies.

The recombinant PtAsp2like1 was found to thermostable and alkalistable. The reported archaeal ASNase showed the optimum pH in the alkaline pH range and optimum activity at high temperatures.[34,37,40]

A gradual increase in enzyme activity was observed from 30 to 80 °C with the optimum at 80 °C. The enzyme activity at 30 and 40 °C was significantly less compared to that at 80 °C. This study was targeted to find asparaginases that can be used in cancer therapy, but PtAsp2like1 did not show high enzyme activity in pharmacologically relevant conditions. The Km of the PtAsp2like1 toward substrate L-asparagine was calculated to be 11.69 mM, which was similar to the other archaeon L-asparaginases *Thermococcus gammatolerans* EJ3 (Km 10.0 mM)[37] and *Pyrococcus furiosus* DSM 3638 (Km 12 mM).[34] The kcat ($5.6 \times 10-2\ s^{-1}$) catalytic efficiency of PtAsp2like1 was significantly less toward substrate L-asparagine (0.47×10^{-2}) compared to other archaeal asparaginases from

https://doi.org/10.1021/acsomega.2c01127
ACS Omega 2022, 7, 40750−40765

Thermococcus. kodakaraensis L-asparaginase (254 mM^{-1} s^{-1}),[40] *Pyrococcus furiosus* DSM 3638 (72.5 mM^{-1} s^{-1}),[34] and *Thermococcus gammatolerans* EJ3 (572.1 mM^{-1} s^{-1}).[37] As compared to the commercial asparaginases, PtAsp2like1 exhibited a very high Km, pointing to the major drawback of its application in cancer therapy.

5. CONCLUSIONS

We have analyzed ASNases from 176 completely sequenced archaeal organisms. A total of 116 homologs of ASNase were obtained from 86 archaeal organisms that segregated into Asp1, Asp2, IaaA, Asp2like1, and Asp2like2 families based on the conserved domain present. The phylogenetic analysis revealed that archaeal ASNases evolved differently from bacterial and eukaryotic ASNases and diversified into five different families. Amino acid sequence alignment and motif analysis divided the archaeal ASNases into two groups. One group is Asp1 and Asp2 ASNases, and the other group is IaaA, Asp2like2, and Asp2like1. Group 1 ASNases were different from group 2 in terms of their structure, active site residues, and conformation of substrate binding cavity. The other two novel putative archaeal families, Asp2like1 and Asp2like2, are completely uncharacterized with no information about their function and mechanism of action. Circular dichroism spectroscopy studies at different temperatures showed that the secondary structure of PtAsp2like1 remained stable up to 70 °C, and on further increase in temperature, structural changes in protein were observed with the complete unfolding of the protein at 90 °C. The temperature-mediated unfolding of protein was irreversible as the native structure of the protein was not regained on cooling. Steady-state fluorescence studies showed a gradual decrease in the fluorescence intensity on increasing the temperature from 30 to 90 °C. PtAsp2like1 was found to be stable in the pH range of 4 to 11 as monitored through far-UV and steady-state fluorescence spectroscopy. Lower concentrations of Gdn-HCl and urea in the range of 0.1 to 0.5 M stabilized the secondary structure of the protein, while at higher Gdn-HCl (range of 2 to 7 M) and urea concentrations (range of 4 to 8 M), the unfolding of protein was observed through far-UV and steady-state fluorescence spectroscopy. PtAsp2like1 is a thermostable and alkali-stable ASNase and displayed optimum activity at 80 °C and pH 10.0. PtAsp2like1 did not show high enzyme activity in pharmacologically relevant conditions. It is a glutaminase-free L-ASNase as it displayed negligible activity when L-glutamine was used as a substrate, the desired property of an enzyme to be used in cancer therapy. The kinetic studies of PtAsp2like1 showed that compared to commercially available bacterial asparaginases, the Km of PtAsp2like1 asparaginase is high and the kcat and catalytic efficiency are very low, indicating that this enzyme is not a suitable candidate for cancer therapy.

As our *in silico* studies showed that Asp2like1, Asp2like2, and IaaA are structurally similar to each other, we can conclude that the probability of finding an asparaginase with desired properties suitable for cancer therapy from these three families is low. The Asp1 family asparaginases from archaea are already reported in the literature and are not found suitable for application in cancer therapy. The results from this study may be used to conclude that the probability of finding therapeutically relevant asparaginases from archaea may be enhanced by focusing efforts on the investigation of the Asp2 family of archaeal asparaginases. This draws attention to the need to investigate ASNase from archaea for future prospects and increases our understanding of new archaeal ASNase families.

■ ASSOCIATED CONTENT

Supporting Information

The Supporting Information is available free of charge at https://pubs.acs.org/doi/10.1021/acsomega.2c01127.

Phylogenetic tree representation of ASNase; sequence alignment of archaeal ASNase representatives from five different families; purification of PtAsp2like1; temperature- and pH-mediated unfolding of PtAsp2like1; Gdn-HCl- and urea-mediated unfolding of PtAsp2like1 studied using CD spectroscopy; Gdn-HCl- and urea-mediated unfolding of PtAsp2like1 studied using fluorescence spectroscopy; structurally characterized ASNase from bacteria, archaea, and eukaryotes homolog; distribution of 116 ASNase homologs from 86 archaeal organisms into different families; the amino acid sequence identity among selected archaeal ASNase representatives from five different families; and the structural similarity between selected archaeal ASNase representatives from five different families based on RMSD values (PDF)

■ AUTHOR INFORMATION

Corresponding Author

Manisha Goel − *Department of Biophysics, University of Delhi South Campus, New Delhi 110021, India;* orcid.org/0000-0002-5135-3696; Phone: 091-11-32216362; Email: manishagoel@south.du.ac.in

Authors

Archana Sharma − *Department of Biophysics, University of Delhi South Campus, New Delhi 110021, India*

Vineeta Kaushik − *Department of Biophysics, University of Delhi South Campus, New Delhi 110021, India*

Complete contact information is available at: https://pubs.acs.org/10.1021/acsomega.2c01127

Author Contributions

#Equal contribution by A.S. and V.K.

Notes

The authors declare no competing financial interest.

■ ACKNOWLEDGMENTS

Dr. Archana Sharma gratefully acknowledges the Research Associate fellowship (5/3/8/39/ITR-F/2018-ITR) received from the Indian Council of Medical Research, Government of India, for supporting this work.

■ REFERENCES

(1) Verma, N.; Kumar, K.; Kaur, G.; Anand, S. L-asparaginase: A promising chemotherapeutic agent. *Crit. Rev. Biotechnol.* **2007**, *27*, 45−62.

(2) Hendriksen, H. V.; Kornbrust, B. A.; Østergaard, P. R.; Stringer, M. A. Evaluating the potential for enzymatic acrylamide mitigation in a range of food products using an asparaginase from *Aspergillus oryzae*. *J. Agric. Food Chem.* **2009**, *57*, 4168−4176.

(3) Kornbrust, B.A.; Stringer, M.A.; Lange, N.E.K.; Hendriksen, H.V.; Whitehurst, R.; Oort, Mv. Asparaginase—an enzyme for acrylamide reduction in food products. In: *Enzymes in Food Technology*.; 2nd edn. Wiley-Blackwell: UK.; 2009, 59−87.

(4) Zuo, S.; Zhang, T.; Jiang, B.; Mu, W. Recent research progress on microbial L-asparaginases. *Appl. Microbiol. Biotechnol.* **2015**, *99*, 1069−1079.
(5) Avramis, V. I.; Tiwari, P. N. Asparaginase (native ASNase or pegylated ASNase) in the treatment of acute lymphoblastic leukemia. *Int. J. Nanomed.* **2006**, *1*, 241−254.
(6) Pui, C. H.; Evans, W. E. Treatment of acute lymphoblastic leukemia. *N. Engl. J. Med.* **2006**, *354*, 166−178.
(7) Shakambari, G.; Ashokkumar, B.; Varalakshmi, P. L-asparaginase − A promising biocatalyst for industrial and clinical applications. *Biocatal. Agric. Biotechnol.* **2019**, *17*, 213−224.
(8) Qeshmi, F. I.; Homaei, A.; Fernandes, P.; Javadpoure, S. Marine microbial l-asparaginase: biochemistry, molecular approaches and applications in tumor therapy and in food industry. *Microbiol. Res.* **2018**, *208*, 99−112.
(9) Villa, I.; Corada, M.; Bartosek, I. L-Asparaginase effects on inhibition of protein synthesis and lowering of the glutamate content in cultured rat hepatocytes. *Toxicol. Lett.* **1986**, *32*, 235−241.
(10) Avramis, V. I.; Sencer, S.; Periclou, A. P.; Sather, H.; Bostrom, B. C.; Cohen, L. J.; Ettinger, A. G.; Ettinger, L. J.; Franklin, J.; Gaynon, P. S.; Hilden, J. M.; Lange, B.; Majlessipour, F.; et al. A randomized comparison of native *Escherichia coli* asparaginase and polyethylene glycol conjugated asparaginase for treatment of children with newly diagnosed standard-risk acute lymphoblastic leukemia: a Children's Cancer Group study. *Blood* **2002**, *99*, 1986−1994.
(11) Patil, S.; Coutsouvelis, J.; Spencer, A. Asparaginase in the management of adult acute lymphoblastic leukaemia: is it used appropriately? *Cancer Treat. Rev.* **2011**, *37*, 202−207.
(12) Reiff, A.; Zastrow, M.; Sun, B. C.; Takei, S.; Mitsuhada, H.; Bernstein, B.; Durden, D. L. Treatment of collagen induced arthritis in DBA/1 mice with l-asparaginase. *Clin. Exp. Rheumatol.* **2001**, *19*, 639−646.
(13) Baruch, M.; Belotserkovsky, I.; Hertzog, B. B.; Ravins, M.; Dov, E.; McIver, K. S.; Breton, Y. S. L.; Zhou, Y.; Cheng, C. Y.; Chen, C. Y.; Hanski, E. An extracellular bacterial pathogen modulates host metabolism to regulate its own sensing and proliferation. *Cell* **2014**, *156*, 97−108.
(14) Sanches, M.; Krauchenco, K.; Polikarpov, I. Structure substrate complexation and reaction mechanism of bacterial asparaginases. *Curr. Chem. Biol.* **2001**, *1*, 175−186.
(15) De Bont, J. M.; van der Holt, B.; Dekker, A. W.; et al. Significant difference in outcome for adolescents with ALL treated on pediatric vs adult protocols in the Netherlands. *Leukemia* **2004**, *18*, 2032−2035.
(16) Fu, C. H.; Sakamoto, K. M. PEG asparaginases. *Expert Opin. Pharmacother.* **2007**, *8*, 1977−1984.
(17) Dinndorf, P. A.; Gootenberg, J.; Cohen, M. H.; et al. FDA drug approval summary: pegaspargase (Oncaspar) for the first-line treatment of children with acute lymphoblastic leukemia (ALL). *Oncologist* **2007**, *12*, 991−998.
(18) Maloney, K. W. Erwinia asparaginase: coming closer to an understanding of its use in pediatric acute lymphoblastic leukemia? *Pediatr Blood Cancer.* **2010**, *54*, 189−190.
(19) Pieters, R.; Hunger, S. P.; Boos, J.; et al. L-asparaginase treatment in acute lymphoblastic leukemia. *Cancer.* **2011**, *117*, 238−249.
(20) Lopes, A. M.; de Oliveira-Nascimento, L.; Ribeiro, A.; Tairum, C. A.; Breyer, C. A.; de Oliveira, M. A.; Monteiro, G.; Souza-Motta, C. M. .; Magalhães, P. . O.; Avendaño, J. G. F.; Cavaco-Paulo, A. M.; Mazzola, P. G.; Rangel-Yagui, C. . O.; Sette, L. D.; Converti, A.; Pessoa, A. Therapeutic l-asparaginase: upstream.; downstream and beyond. *Crit. Rev. Biotechnol* **2017**, *37*, 82−99.
(21) Zalipsky, S. Chemistry of polyethylene glycol conjugates with biologically active molecules. *Adv. Drug Delivery Rev.* **1995**, *16*, 157−182.
(22) Harris, J. M.; Chess, R. B. Effect of pegylation on pharmaceuticals. *Nat. Rev. Drug Discovery* **2003**, *2*, 214−221.
(23) Santos, J. H.; Flores-Santos, J. C.; Meneguetti, G. P.; Rangel-Yagui, C. O.; Coutinho, J. A.; Vitolo, M.; Ventura Sonia, P. M.; Pessoa, A., Jr. In situ purification of periplasmaticL-asparaginase by aqueous two-phase systems with ionic liquids (ILs) asadjuvants. *J. Chem. Technol. Biotechnol.* **2018**, *93*, 1871−1880.
(24) Carter, M. C.; Meyerhoff, M. E. Instability of succinyl ester linkages in O2 -monosuccinyl cyclic AMP-protein conjugates at neutral pH. *J. Immunol. Methods* **1985**, *81*, 245−257.
(25) Brumano, L. P.; da Silva, F. V. S.; Costa-Silva, T. A.; Apolinário, A. C.; Santos, J. H. P. M.; Kleingesinds, E. K.; Monteiro, G.; Rangel-Yagui, C. O.; Benyahia, B.; Junior, A. P. Development of L-Asparaginase biobetters: Current research status and review of the desirable quality profiles. *Front Bioeng. Biotechnol.* **2019**, *6*, 212.
(26) Nguyen, H. A.; Su, Y.; Lavie, A. Structural Insight into Substrate Selectivity of *Erwinia chrysanthemi* L-Asparaginase. *Biochemistry* **2016**, *55*, 1246−1253.
(27) Loureiro, C. B.; Borges, K. S.; Andrade, A. F.; Tone, L. G.; Said, S. Purification and biochemical characterization of native and pegylated form of l-asparaginase from *Aspergillus terreus* and evaluation of its antiproliferative activity. *Adv. Microbiol.* **2012**, *02*, 138−145.
(28) Ardalan, N.; Mirzaie, S.; Sepahi, A. A.; Khavari-Nejad, R. A. Novel mutant of *Escherichia coli* asparaginase II to reduction of the glutaminase activity in treatment of acute lymphocytic leukemia by moleculardynamics simulations and QM-MM studies. *Med. Hypotheses.* **2018**, *112*, 7−17.
(29) Michalska, K.; Bujacz, G.; Jaskolski, M. Crystal Structure of Plant Asparaginase. *J. Mol. Biol.* **2006**, *360*, 105−116.
(30) Willis, R. C.; Woolfolk, C. A. Asparagine utilization in *Escherichia coli*. *J. Bacteriol.* **1974**, *118*, 231−241.
(31) Ho, D. H.; Whitecar, J. P., Jr.; Luce, J. K.; Frei, E., 3rd L-asparagine requirement and the effect of L-asparaginase on the normal and leukemic human bone marrow. *Cancer Res.* **1970**, *30*, 466−472.
(32) El-Naggar, N. E.-A.; El-Ewasy, S.; El-Shweihy, N. M. Microbial L-asparaginase as a Potential Therapeutic Agent for the Treatment of Acute Lymphoblastic Leukemia: The Pros and Cons. *Int. J. Pharmacol.* **2014**, *10*, 182−199.
(33) Yao, M.; Yasutake, Y.; Morita, H.; Tanaka, I. Structure of the type I L-asparaginase from the hyperthermophilic archaeon *Pyrococcus horikoshii* at 2.16 AE resolution. *Acta Crystallogr.* **2005**, *D61*, 294−301.
(34) Bansal, S.; Gnaneswari, D.; Mishra, P.; Kundu, B. Structural stability and functional analysis of L-asparaginase from *Pyrococcus furiosus*. *Biochemistry-Moscow.* **2010**, *75*, 375−381.
(35) Bansal, S.; Srivastava, A.; Mukherjee, G.; Pandey, R.; Verma, A. K.; Mishra, P.; Kundu, B. Hyperthermophilic asparaginase mutants with enhanced substrate affinity and antineoplastic activity: structural insights on their mechanism of action. *FASEB J.* **2012**, *26*, 1161−1171.
(36) Chohan, S. M.; Rashid, N. TK1656.; a thermostable L-asparaginase from *Thermococcus kodakaraensis*.; exhibiting highest ever reported enzyme activity. *J. Biosci. Bioeng.* **2013**, *116*, 438−443.
(37) Zuo, S.; Xue, D.; Zhang, T.; Jiang, B.; Mu, W. Biochemical characterization of an extremely thermostable L-asparaginase from *Thermococcus gammatolerans* EJ3. *J. Mol. Catal. B: Enzym.* **2014**, *109*, 122−129.
(38) Tomar, R.; Garg, D. K.; Mishra, R.; Thakur, A. K.; Kundu, B. N-terminal domain of *Pyrococcus furiosus* l-asparaginase functions as a non-specific.; stable.; molecular chaperone. *FEBS J.* **2013**, *280*, 2688−2699.
(39) Tomar, R.; Sharma, P.; Srivastava, A.; Bansal, S.; Kundu, B. Structural and functional insights into an archaeal L-asparaginase obtained through the linker-less assembly of constituent domains. *Acta Crystallogr., Sect. D: Biol. Crystallogr.* **2014**, *70*, 3187−3197.
(40) Guo, J.; Coker, A. R.; Wood, S. P.; Cooper, J. B.; Chohan, S. M.; Rashid, N.; Akhtar, M. Structure and function of the thermostable L-asparaginase from *Thermococcus kodakarensis*. *Acta Crystallogr.* **2017**, *D73*, 889−895.
(41) Altschul, S. F.; Gish; Miller, W.; Myers, E. W.; Lipman, D. J. Basic local alignment search tool. *J. Mol. Biol.* **1990**, *5*, 403−410.

https://doi.org/10.1021/acsomega.2c01127
ACS Omega 2022, 7, 40750−40765

(42) Lu, S.; et al. CDD/SPARCLE: the conserved domain database in 2020. *Nucleic Acids Res.* **2020**, *48*, 265−268.
(43) Huang, Y.; Niu, B.; Gao, Y.; Fu, L.; Li, W. CD-HIT Suite: a web server for clustering and comparing biological sequences. *Bioinformatics* **2010**, *1*, 680−682.
(44) Sievers, F.; Wilm, A.; Dineen, D.; Gibson, T. J.; Karplus, K.; Li, W.; Lopez, R.; William, H. M.; Remmert, M.; Soding, J.; Thompson, J. D.; Higgins, D. G. Fast.; scalable generation of high-quality protein multiple sequence alignments using Clustal Omega. *Mol. Syst. Biol.* **2011**, 1−6.
(45) Tamura, K.; Stecher, G.; Peterson, D.; Filipski, A.; Kumar, S. MEGA6: Molecular Evolutionary Genetics Analysis Version 6.0. *Mol. Biol. Evol.* **2013**, *30*, 2725−2729.
(46) Notredame, C.; Higgins, D. G.; Heringa, J. T-Coffee: A Novel Method for Fast and Accurate Multiple Sequence Alignment. *J. Mol. Biol.* **2000**, *302*, 205−217.
(47) Bailey, T. L.; Bodén, M.; Buske, F. A.; Frith, M.; Grant, C. E.; Clementi, L.; Ren, J.; Li, W. W.; William, S. N. MEME SUITE: tools for motif discovery and searching. *Nucleic Acids Res.* **2009**, *37*, 202−208.
(48) Waterhouse, A.; Bertoni, M.; Bienert, S.; Studer, G.; Tauriello, G.; Gumienny, R.; Heer, F. T.; de Beer, T. A. P.; Rempfer, C.; Bordoli, L.; Lepore, R.; Schwede, T. SWISS-MODEL: homology modelling of protein structures and complexes. *Nucleic Acids Res.* **2018**, *46*, 296−303.
(49) Lubkowski, J.; Wlodawer, A. Geometric considerations support the double-displacement catalytic mechanism of l-asparaginase. *Protein Sci.* **2019**, *28*, 1850−1864.
(50) Nomme, J.; Su, Y.; Konrad, M.; Lavie, A. Structures of apo and product-bound human L-asparaginase: insights into the mechanism of autoproteolysis and substrate hydrolysis. *Biochemistry* **2012**, *28*, 6816−6826.
(51) Michalska, K.; Hernandez-Santoyo, A.; Jaskolski, M. The Mechanism of Autocatalytic Activation of Plant-type L-Asparaginases. *J. Biol. Chem.* **2008a**, *283*, 13388−13397.
(52) Michalska, K.; Borek, D.; Hernandez-Santoyo, A.; Jaskolski, M. Crystal packing of plant-type L-asparaginase from *Escherichia coli*. *Acta Crystallogr., Sect. D: Biol. Crystallogr.* **2008b**, *64*, 309−320.
(53) DeLano, W. L. Pymol: An open-source molecular graphics tool. *CCP4 Newsl. Protein Crystallogr* **2002**, *40*, 82−92.
(54) Derst, C.; Henseling, J.; Röhm, K.-H. Engineering the substrate specificity of *Escherichia coli* asparaginase II. Selective reduction of glutaminase activity by amino acid replacements at position 248. *Protein Sci.* **2000**, *9*, 2009−2017.
(55) Nomme, J.; Su, Y.; Lavie, A. Elucidation of the Specific Function of the Conserved Threonine Triad Responsible for Human l-Asparaginase Autocleavage and Substrate Hydrolysis. *J. Mol. Biol.* **2014**, *426*, 2471−2485.
(56) Michalska, K.; Brzezinski, K.; Jaskolski, M. Crystal Structure of Isoaspartyl Aminopeptidase in Complex with L-Aspartate. *J. Biol. Chem.* **2005**, *280*, 28484−28491.
(57) R Core Team. *R: A language and environment for statistical computing*. R Foundation for Statistical Computing: Vienna, Austria. 2020. URLhttps://www.R-project.org/.
(58) Swain, A. L.; Jaskolski, M.; Housset, D.; Rao, M.; Wlodawer, A. Crystal structure of *Escherichia coli* L-asparaginase.; an enzyme used in cancer therapy. *Proc. Natl. Acad. Sci. U. S. A.* **1993**, *90*, 1474−1478.
(59) Miller, M.; Rao, J. K.; Wlodawer, A.; Gribskov, M. R. A left-handed crossover involved in amidohydrolase catalysis Crystal structure of *Erwinia chrysanthemi* L-asparaginase with bound L-aspartate. *FEBS Lett.* **1993**, *328*, 275−279.
(60) Borek, D.; Jaskólski, M. Sequence analysis of enzymes with asparaginase activity. *Acta Biochim. Pol.* **2001**, *48*, 893−902.
(61) Kravchenko, O. V.; Kislitsin, Y. A.; Popov, A. N.; Nikonov, S. V.; Kuranova, I. P. Three-dimensional structures of L-asparaginase from *Erwinia carotovora* complexed with aspartate and glutamate. *Acta Crystallogr., Sect. D: Biol. Crystallogr.* **2008**, *64*, 248−256.
(62) Schalk, A. M.; Lavie, A. Structural and Kinetic Characterization of Guinea Pig l-Asparaginase Type III. *Biochemistry* **2014**, *53*, 2318−2328.
(63) Saeed, H.; Ali, H.; Soudan, H.; Embaby, A.; EL-Sharkawy, A.; Farag, A.; Hussein, A.; Ataya, F. Molecular cloning.; structural modeling and production of recombinant *Aspergillus terreus* l-asparaginase in *Escherichia coli*. *Int. J. Biol. Macromol.* **2017**, *106*, 1041−1051.
(64) Lubkowski, J.; Palm, G. J.; Gilliland, G. L.; Derst, C.; Röhm, K. H.; Wlodawer, A. Crystal structure and amino acid sequence of *Wolinella succinogenes* L-asparaginase. *Eur. J. Biochem.* **1996**, *1*, 201−207.
(65) Bhuyan, A. K. Protein stabilization by urea and guanidine hydrochloride. *Biochemistry* **2002**, *41*, 13386−13394.
(66) Ortlund, E.; Lacount, M. W.; Lewinski, K.; Lebioda, L. Reactions of *Pseudomonas* 7A glutaminase-asparaginase with diazo analogues of glutamine and asparagine result in unexpected covalent inhibitions and suggests an unusual catalytic triad Thr-Tyr-Glu. *Biochemistry* **2000**, *39*, 1199−1204.
(67) Aung, H.-P.; Bocola, M.; Schleper, S.; Klaus-Heinrich, R. Dynamics of a mobile loop at the active site of *Escherichia coli* asparaginase. *Biochim. Biophys. Acta, Protein Struct. Mol. Enzymol.* **2000**, *1481*, 349−359.
(68) Sanches, M.; Krauchenco, S.; Polikarpov, I. Structure.; Substrate Complexation and Reaction Mechanism of Bacterial Asparaginases. *Curr. Chem. Biol.* **2007**, *1*, 75−86.
(69) Brannigan, J. A.; Dodson, G.; Duggleby, H. J.; Moody, P. C.; Smith, J. L.; Tomchick, D. R.; Murzin, A. G. A protein catalytic framework with an N-terminal nucleophile is capable of self-activation. *Nature* **1995**, *378*, 416−419.
(70) Cantor, J. R.; Stone, E. M.; Chantranupong, L.; Georgiou, G. The human asparaginase-like protein 1hASRGL1 is an Ntn hydrolase with beta-aspartyl peptidase activity. *Biochemistry* **2009**, *48*, 11026−11031.
(71) Offman, M. N.; Krol, M.; Patel, N.; Krishnan, S.; Liu, J.; Saha, V.; Bates, P. A. Rational engineering of L-asparaginase reveals importance of dual activity for cancer cell toxicity. *Blood* **2011**, *117*, 1614−1621.
(72) Mehta, R. K.; Verma, S.; Pati, R.; Sengupta, M.; Khatua, B.; Jena, R. K.; et al. Mutations in subunit interface and B-cell Epitopes improve Antileukemic activities of *Escherichia coli* asparaginase-II: evaluation of immunogenicity in mice. *J. Biol. Chem.* **2014**, *289*, 3555−3570.
(73) Blattner, F. R.; Plunkett, G., 3rd.; Bloch, C. A.; Perna, N. T.; Burland, V.; Riley, M.; Collado-Vides, J.; Glasner, J. D.; Rode, C. K.; Mayhew, G. F.; Gregor, J.; Davis, N. W.; Kirkpatrick, H. A.; Goeden, M. A.; Rose, D. J.; Mau, B.; Shao, Y. The complete genome sequence of *Escherichia coli* K-12. *Science* **1997**, *5*, 1453−1462.
(74) Borek, D.; Podkowinski, J.; Kisiel, A.; Jaskolski, M. Isolation and characterization of cDNAencoding L-asparaginase from *Lupinus luteus* (Accession No. AF112444). (PGR99-050). *Plant Physiol.* **1999**, *119*, 1568.
(75) Futterer, O.; Angelov, A.; Liesegang, H.; Gottschalk, G.; Schleper, C.; Schepers, B.; Dock, C.; Antranikian, G.; Liebl, W. Genome sequence of *Picrophilus torridus* and its implications for life around pH 0. *Proc. Natl. Acad. Sci. U. S. A.* **2004**, *101*, 9091−9096.
(76) Valeur, B. *Molecular Fluorescence: Principles and Applications*, WILEY-VCH Verlag GmbH , 2001, DOI: 10.1002/3527600248.

https://doi.org/10.1021/acsomega.2c01127
ACS Omega 2022, 7, 40750−40765